HHS Public Access

Author manuscript

Cell Stem Cell. Author manuscript; available in PMC 2024 December 07.

Published in final edited form as:

Cell Stem Cell. 2023 December 07; 30(12): 1640–1657.e8. doi:10.1016/j.stem.2023.10.008.

VEGFA mRNA-LNP promotes biliary epithelial cell-to-hepatocyte conversion in acute and chronic liver diseases and reverses steatosis and fibrosis

Fatima Rizvi[1], **Yu-Ri Lee**[2], **Ricardo Diaz-Aragon**[3], **Pushpinder S. Bawa**[1], **Juhoon So**[2], **Rodrigo M. Florentino**[3], **Susan Wu**[1], **Arianna Sarjoo**[1], **Emily Truong**[1], **Anna R. Smith**[1], **Feiya Wang**[1], **Elissa Everton**[1], **Alina Ostrowska**[3], **Kyounghwa Jung**[2], **Ying Tam**[4], **Hiromi Muramatsu**[5], **Norbert Pardi**[5], **Drew Weissman**[6], **Alejandro Soto-Gutierrez**[3], **Donghun Shin**[2], **Valerie Gouon-Evans**[1,7,*]

[1]Center for Regenerative Medicine, Department of Medicine, Section of Gastroenterology, Boston University and Boston Medical Center, Boston, MA 02118, USA

[2]Department of Developmental Biology, Pittsburgh Liver Research Center, McGowan Institute for Regenerative Medicine, University of Pittsburgh School of Medicine, Pittsburgh, PA 15260, USA

[3]Department of Pathology, Center for Transcriptional Medicine, Pittsburgh Liver Research Center, McGowan Institute for Regenerative Medicine, University of Pittsburgh School of Medicine, Pittsburgh, PA 15213, USA

[4]Acuitas Therapeutics, Vancouver, BC, V6T 1Z3, Canada

[5]Department of Microbiology, Perelman School of Medicine, University of Pennsylvania, Philadelphia, PA 19104, USA

[6]Department of Medicine, Infectious Diseases Division, Perelman School of Medicine, University of Pennsylvania, Philadelphia, PA 10104, USA

[*]Correspondence should be addressed to VG-E: valerige@bu.edu.

Author contributions

FR conducted the experiments, designed the experiments and wrote the paper. Y-RL, RD-A, JS, RMF, SW, AS, ARS, EE, and AO conducted and designed experiments. PSB and FW analyzed scRNA Seq data. HM, NP and DW designed and provided mRNA. YT provided mRNA-LNP. AS-G, DS and VG-E designed and supervised experiments. DS and VG-E wrote the paper. All authors edited the paper. VG-E led the study.

Declaration of interests

In accordance with the University of Pennsylvania policies and procedures and our ethical obligations as researchers, we report that DW is named on patents that describe the use of nucleoside-modified mRNA as a platform to deliver therapeutic proteins. DW and NP are also named on a patent describing the use of modified mRNA in lipid nanoparticles. DW, NP and VG-E are named on a patent describing the use of nucleoside modified mRNA in lipid nanoparticles to treat liver diseases. DW, RD-A, RMF, AO and AS-G have a provisional international patent application that describes the use of nucleoside modified mRNA in lipid nanoparticles to treat liver diseases. DW, AO and AS-G are co-founders and have a financial interest in Pittsburgh ReLiver Inc.

Supplemental Information

Document S1: Figures S1 to S7

Table S1: Human tissue samples for histology evaluation, or gene and protein expression analysis.

Table S2: DNA sequences used as template to in vitro transcribe nucleoside modified mRNA.

Table S3: Primer list for qRT-PCR, related to STAR Methods

[7]Lead contact

Summary

The liver is known for its remarkable regenerative ability through proliferation of hepatocytes. Yet, during chronic injury or severe hepatocyte death, proliferation of hepatocytes is exhausted. To overcome this hurdle, we propose vascular-endothelial-growth-factor A (VEGFA) as a therapeutic means to accelerate biliary epithelial cell (BEC)-to-hepatocyte conversion. Investigation in zebrafish establishes that blocking VEGF receptors abrogates BEC-driven liver repair, while VEGFA overexpression promotes it. Delivery of VEGFA via non-integrative and safe nucleoside-modified mRNA encapsulated into lipid-nanoparticles (mRNA-LNP) in acutely or chronically injured mouse livers induces robust BEC-to-hepatocyte conversion and elimination of steatosis and fibrosis. In human and murine diseased livers, we further identified VEGFA-receptor KDR-expressing BECs associated with KDR-expressing cell-derived hepatocytes. This defines KDR-expressing cells, most likely being BECs, as facultative progenitors. This study reveals unexpected therapeutic benefits of VEGFA delivered via nucleoside-modified mRNA-LNP, whose safety is widely validated with COVID-19 vaccines, for harnessing BEC-driven repair to potentially treat liver diseases.

Graphical Abstract

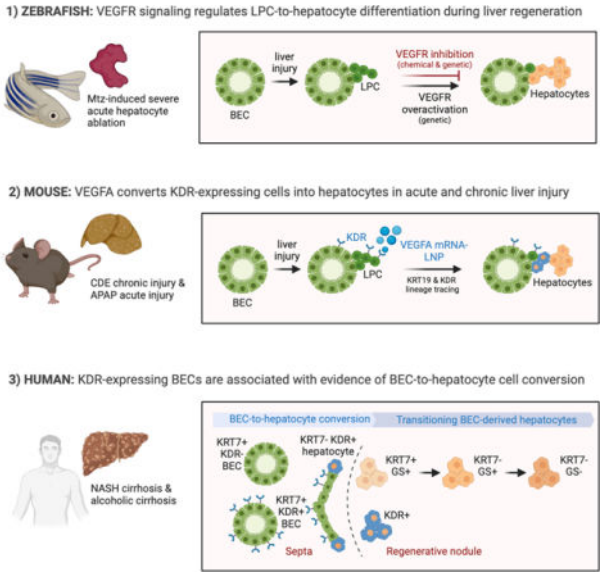

ETOC

In this issue of *Cell Stem Cell*, Rizvi et al. reveal the therapeutic impact of VEGFA delivered via the safe mRNA-LNP platform, widely developed for COVID-19 vaccines, in promoting BEC-to-hepatocyte conversion in acute and chronic murine liver diseases, and in reversing steatosis and fibrosis, two hallmarks of human liver diseases.

Keywords

BEC-driven liver regeneration; VEGFA mRNA-LNP; KDR; acute liver injury; chronic liver injury; ductular reaction; BEC-derived intermediate liver progenitor cells; human liver cirrhosis

Introduction

Mortality related to end stage liver disease (ESLD) is ranked as the 12th most common cause of death in the US. Liver transplantation remains the only treatment for ESLD, but this procedure is critically challenged by the shortage of organ donors. The remarkable ability of the liver to regenerate by proliferation of hepatocytes is well documented[1], yet in the case of severe acute hepatocyte death or chronic ESLD, proliferation of mature cells becomes exhausted[2,3] due to the escalating progression of steatosis, inflammation, fibrosis and cirrhosis. In these cases, the presence of alternative precursors of hepatocytes that derive from biliary epithelial cells (BECs) has been postulated, and these cells have been referred to by various names, including intermediate liver progenitor cells (LPCs)[4]. Expansion of LPCs, a process described as ductular reaction (DR), is present in virtually all chronic and acute human liver diseases, suggesting an alternative regeneration process by which BECs proliferate and differentiate into hepatocytes, the BEC-driven liver regeneration[5–15]. The evidence for the contribution of BECs to de novo hepatocytes in humans is illustrated by the presence of hepatocytes expressing the BEC marker EpCAM emerging from highly proliferative DR areas in advanced cirrhotic livers[16], detection of “bi-phenotypic cells”[17] or “ductular hepatocytes”[18] positive for both the BEC marker KRT19 and the hepatocyte marker HNF4A[17] or HepPar1 antigen[18], and observation of budding of hepatocyte-like cells expressing the hepatocytic marker glutamine synthetase (GS) from BECs within DRs[19–23]. Specifically, Stueck and colleagues have quantified the emerging immature hepatocytes budding from KRT19+ BECs within the septa developed in human cirrhotic livers, and estimated that they represented up to 70% of hepatocytes[19]. Importantly, a recent study showed that aberrant GS positivity adjacent to portal tracts is significantly associated with regressed cirrhosis in humans[24], suggesting the clinical benefit of LPC-derived hepatocytes in resolving human cirrhosis. In an attempt to lineage trace the LPCs within DRs in human cirrhotic livers, Lin and colleagues have used mutational analysis in mitochondrial DNA encoding cytochrome c oxidase enzyme, and showed the descent of hepatocytes within monoclonal regenerative nodules from adjacent LPC-associated DRs[25]. Consistent with an alternative BEC-mediated liver repair identified in human liver diseases, the BEC origin of de novo hepatocytes has been demonstrated in lineage tracing mouse models in which hepatocyte proliferation was significantly impaired by lack of Mdm2[26], deficiency in β1 integrin[27] or β-catenin[28], overexpression of p21 in hepatocytes[27], or following long-term chronic injuries[17,29]. In these studies, percentages of hepatocytes mapped from BECs averaged 15%[27,28]. In the same line of evidence, our lineage tracing studies in zebrafish as well as others robustly demonstrated the BEC origin of the majority of hepatocytes after near complete ablation of hepatocytes[30–32].

This emerging literature raises the exciting possibility that BECs could be harnessed for therapeutic purposes to produce de novo hepatocytes and restore liver function. The current

limitation for the efficient therapeutic use of BECs is the lack of druggable pathways that efficiently trigger the BEC-to-hepatocyte conversion. In this study, we propose that VEGFA promotes BEC-to-hepatocyte conversion and rescues liver function using complementary mouse and zebrafish liver injury models. Although VEGFA signaling is a known master regulator of angiogenesis, previous studies provide evidence for its role in improving liver regeneration after injury in rodents[33–36]. The last two studies indicated that VEGFA binds KDR expressed on liver sinusoidal endothelial cells that in turn secrete hepatocyte mitogens, thereby promoting the proliferation of hepatocytes. The role of VEGFA in accelerating BEC-driven regeneration was suggested in a rat injury model in which hepatocyte proliferation was compromised[37]; however, it is not known yet if VEGFA promotes BEC-to-hepatocyte conversion. A direct effect of VEGFA on the BEC lineage is possible as KDR is expressed in BECs following liver injury in rats[38], in developing BECs generated from human induced pluripotent stem cells[39], and in ductal plates in the developing human fetal biliary system[40]. Interestingly, our previous studies using embryonic stem cell differentiation cultures identified a liver progenitor cell expressing KDR whose differentiation into hepatocyte-like cells was inhibited when KDR signaling was chemically abrogated[41]. These data suggested an unexpected role for the ligand VEGFA to promote hepatocyte fate decision from a KDR-expressing precursor. Here, our complementary zebrafish and mouse lineage tracing models supported by analyses of human ESLD specimens reveal that VEGFA, delivered with the clinically safe and non-integrative lipid nanoparticle-encapsulated nucleoside-modified mRNA (mRNA-LNP) platform[42], induces BEC-to-hepatocyte differentiation through cell conversion of KDR-expressing BECs acting as facultative liver progenitor cells and mitigates the liver disease in mice. This study uncovers an unprecedented application of mRNA-LNP for tissue regeneration that departs from its original applications as protein replacement or immunization.

Results

VEGFR signaling regulates BEC-to-hepatocyte conversion during liver regeneration in zebrafish

To investigate the molecular mechanisms underlying BEC-driven liver regeneration, we previously performed a chemical screen[43] using the zebrafish hepatocyte ablation model, *Tg(fabp10a:CFP-NTR)*^{s931}, in which metronidazole (Mtz) treatment specifically ablates all nitroreductase (NTR)-expressing hepatocytes, thereby eliciting BEC-driven liver regeneration[31]. Through this screen, we reported that suppressing VEGFR signaling with two VEGFR inhibitors, SU5416[44] and SU4312[45], significantly reduced the size of regenerating livers but did not affect the induction of early hepatocyte markers Prox1 and Hnf4a in BEC-derived LPCs[43], suggesting normal BEC-to-LPC dedifferentiation. We here sought to determine whether VEGFR signaling regulates the next step in BEC-driven liver regeneration, LPC-to-hepatocyte differentiation. To distinguish BEC-derived hepatocytes, we used a Notch zebrafish reporter line, *Tg(Tp1:H2B-mCherry)*^{s939}, which expresses histone 2B (H2B) and mCherry fusion proteins in BECs[31]. A long half-life of H2B-mCherry allows for tracing the lineage of BECs; thus, BECs are strong H2B-mCherry+ and BEC-derived hepatocytes are weak H2B-mCherry+[31]. Treating *Tg(fabp10a:CFP-NTR)* larvae with SU5416 from ablation 18 hours (A18h) to regeneration 24 hours (R24h)

significantly reduced the size of regenerating livers (Figure 1A), as reported[43]. Importantly, the SU5416 treatment greatly suppressed the expression of the hepatocyte marker Bhmt at R24h (Figure 1A), suggesting a defect in LPC-to-hepatocyte differentiation. This defect was confirmed with two additional hepatocyte markers, *gc* and *f5* (Figure 1B) and with a selective VEGFR2 inhibitor, ZM323881 hydrochloride[46] (Figure S1A and S1B). To determine if VEGFR inhibition also affects LPC-to-BEC differentiation, we measured BEC numbers in regenerating livers by counting H2B-mCherry^{strong}/VenusPEST^{strong} double-positive cells. Indeed, the SU5416 treatment reduced BEC number (Figure S1C), indicating that VEGFR inhibition impairs both LPC-to-BEC and LPC-to-hepatocyte differentiation. Thus, it appears that upon VEGFR inhibition, most LPCs failed to differentiate into either hepatocytes or BECs, instead remaining in an undifferentiated state. Given the reduced liver size in SU5416-treated regenerating larvae, we also determined if the small liver was due to enhanced cell death or reduced proliferation or both. LPC proliferation was not reduced (Figure S1D), but its death was significantly increased (Figure S1E), indicating that the small liver in SU5416-treated regenerating larvae is due to enhanced LPC death. Complimentary to the pharmacological inhibition, we genetically blocked VEGFR signaling using the *Tg(hs:sflt1)^{bns80}* line, which expresses a soluble form of VEGFR1 (sFlt1), a decoy receptor for VEGFA, VEGFB, and PlGF[38], upon heat-shock[47]. sFlt1 overexpression also reduced Bhmt expression and liver size in regenerating livers at R26h (Figure 1C), phenocopying the effects of the SU5416 treatment.

Inversely, we next investigated if VEGFR overactivation could promote LPC-to-hepatocyte differentiation. We used the *Tg(hs:loxP-mCherry-loxP-hVEGFA)^{mn32}* line, which expresses human VEGFA$_{165}$ upon heat-shock following Cre-mediated, *mCherry-loxP* excision[48], together with the *Tg(Tp1:CreERT2)^{s959}* line that expresses Cre^{ERT2} in BECs. Larvae were treated with 4-OHT from 2.5 to 3.5 days post-fertilization (dpf) to induce the Cre-mediated excision of *mCherry-loxP* in BECs, heat-shocked twice at A20h and A34h to trigger hVEGFA expression and harvested at R3h. hVEGFA expression in a subset of BEC-derived cells (BECs and LPCs) increased Bhmt expression in regenerating livers at R3h compared with controls (Figure 1D). Additionally, we generated another heat-inducible hVEGFA transgenic line, *Tg(hs:hVEGFA-P2A-Venus)^{pt624}*, which expresses both hVEGFA$_{165}$ and Venus in the entire body upon heat-shock. Using this line, we observed that VEGFA overexpression increased the expression of *gc* and *f5* in regenerating livers at R6h (Figure S1F). These overexpression data suggest that VEGFR overactivation is sufficient to promote LPC-to-hepatocyte differentiation. Altogether, the zebrafish data demonstrate the essential role of VEGFR signaling in BEC-driven liver regeneration, particularly in LPC-to-hepatocyte differentiation.

VEGFA mRNA-LNP induces BEC-to-hepatocyte conversion in CDE diet-induced chronic liver injury in mice and resolves liver damage

We next interrogated the clinical benefit of VEGFR activation in restoring liver function in a chronic liver injury model in mice. To trace hepatocytic fate of BECs, liver injury was induced in *Krt19*-Cre^{ERT},*R26*^{LSL}tdTomato[27] mice with the choline-deficient diet supplemented with ethionine (CDE) following an injection of AAV8-*Tbg*-p21 (CDE/p21 model)[27] (Figure 2A), which recapitulates some key features of the human non-alcoholic

steatohepatitis (NASH) liver disease including steatosis, DR, and fibrosis[27]. Injection of AAV8-*Tbg*-p21 triggered p21 expression in hepatocytes and was used to induce hepatocyte senescence[27,28], a common feature seen in all human chronic liver disease[49,50]. We chose to deliver VEGFA in mice via injection of nucleoside-modified mRNA-LNP allowing controlled transient expression of VEGFA in the liver for better clinical translation. We have recently demonstrated efficacy of mRNA-LNP to transiently express regenerative factors in the liver[51,52] and that their translation into proteins can last a few days, enough time to revert some features of liver diseases[51,52]. For the present study, robust serum levels of VEGFA proteins were detected as early as 5 hours after one intravenous injection of VEGFA mRNA-LNP (Figure 2B). The levels remained high for the following 24 hours, yet rapidly decreased to baseline levels 48 hours later and were weakly detected by 72 hours. This kinetic remained similar during liver injury (Figure 2B). Mice were administered two injections of either VEGFA mRNA-LNP or control LNP (formulated with untranslatable Poly(C) RNA or neutral firefly luciferase-encoding mRNA) after the diet was over. Strikingly, large patches of diffused tdTomato+ clusters appeared in all liver lobes of VEGFA mRNA-LNP-treated mice, representing mostly hepatocytes (Figure 2C, yellow outline; Figure 2D). In contrast, in control LNP-treated mice, tdTomato+ clusters were sporadic and small (Figure 2C, 2D), with the majority composed of BECs (Figure 2D, see numerous * areas). tdTomato+ hepatocytes (Figure 2D, arrowheads) were adjacent to tdTomato+ BECs (Figure 2D, arrows), supporting their BEC origin. Functionally, the tdTomato+ hepatocytes were equally efficient in storing glycogen as the adjacent tdTomato- hepatocytes (Figure 2E), and they expressed the mature markers CPS1, specific for zone 1/2, or GS specific for zone 3, when they reached central vein areas (Figure S2A, arrows). Quantification of tdTomato+ hepatocytes by flow cytometry confirmed that VEGFA mRNA-LNP significantly augment BEC-to-hepatocyte conversion (Figures 2F, S2B). Since the lineage tracing efficiency varies greatly among *Krt19*-Cre^{ERT},*R26*^{LSL}tdTomato mice, the percent labeled BEC population estimated from the non-parenchymal fraction (Figures S2B, S2C) was used to adjust for lineage tracing discrepancy and defined the adjusted % tdTomato+ hepatocytes for each mouse (Figure 2F). We estimated that VEGFA mRNA-LNP promote 5.3-fold greater % tdTomato+ hepatocytes as compared to control LNP-treated mice. In contrast to the reported role of VEGFA in promoting BEC proliferation[38], here the extent of DR was similar between the two groups (Figure S2D), most likely due to greater BEC-to-hepatocyte conversion in VEGFA mRNA-LNP-treated group, as supported by lower density of KRT7+ BECs in areas associated with tdTomato+ hepatocytes (Figure S2E). Importantly, for clinical translation of VEGFA mRNA-LNP, VEGFA-mediated BEC-to-hepatocyte conversion was consistently associated with complete reversion of fibrosis and steatosis (Figure 2G, 2H). In line with increased lipid clearance from treated hepatocytes, serum levels of cholesterol in VEGFA mRNA-LNP-treated groups were significantly higher (Figure S2F). Overall, treatment of the CDE/p21 mouse model with two injections of VEGFA mRNA-LNP fully reverts steatosis and fibrosis, the two key features observed in NASH patients, suggesting a potential clinical benefit of VEGFA mRNA-LNP to alleviate the human NASH disease.

Since numerous reports have shown that BEC-driven liver repair occurs mainly in mouse models in which hepatocyte proliferation was impaired[26–28], we asked whether suppression

of hepatocyte proliferation was a prerequisite for VEGFA mRNA-LNP-mediated BEC-to-hepatocyte conversion. We administered VEGFA mRNA-LNP in CDE-fed mice that were not pre-injected with AAV8-*Tbg*-p21. In both control LNP- and VEGFA mRNA-LNP-treated groups, DR was much lower than in AAV8-*Tbg*-p21 administered mice (Figure S2D vs Figure S2G), indicating that hepatocyte senescence accelerates BEC expansion. Control LNP-treated group did not generate any tdTomato+ hepatocytes as expected[27]. However, we consistently observed emergence of tdTomato+ hepatocytes in VEGFA mRNA-LNP-treated groups (Figure S2H). The tdTomato+ hepatocytes were always adjacent to hepatocytes that naturally induced endogenous p21 expression (Figure S2I, panels 1,2,3). These results demonstrate that p21-mediated suppression of hepatocyte proliferation not only promotes BEC proliferation but also their conversion to hepatocytes. Importantly, VEGFA mRNA-LNP in the presence of hepatocyte proliferation can still trigger BEC-to-hepatocyte conversion, yet combined with suppression of hepatocyte proliferation, potentializes cell conversion to a clinically relevant extent and reverses steatosis and fibrosis.

VEGFA mRNA-LNP promotes BEC-to-hepatocyte conversion in APAP-induced acute liver injury in mice

Given that acute acetaminophen (APAP) toxicity induces DR[53,54], we investigated whether VEGFA mRNA-LNP could also promote generation of de novo hepatocytes from BECs during APAP overdose. If effective, VEGFA mRNA-LNP treatment could serve for the nearly 30% of severe cases of APAP overdose requiring liver transplantation[55] as an alternative treatment to the drug NAC currently used in the clinic to neutralize APAP toxic metabolite NAPQI. Evidence of emergence of intermediate hepatocytes from BECs in severe intoxication in humans has been reported[54], yet the process of BEC-to-hepatocyte conversion must be accelerated to become a viable and effective treatment for acute liver injuries, as proposed here with VEGFA mRNA-LNP. To better reflect clinical cases of human severe acute APAP intoxication in which hepatocyte senescence is consistently observed[54,56], *Krt19*-Cre^{ERT},*R26*^{LSL}tdTomato mice were injected with AAV8-*Tbg*-p21 one week prior to APAP administration (Figure 2I). C57Bl6 mice were used to characterize the liver injury in mice pretreated with AAV-*Tbg*-p21 (Figure S3A). P21 was expressed in nearly 70% of hepatocytes (Figure S3B). Necrosis and cell death were similarly induced 24 hours following APAP overdose in both AAV-*Tbg*-p21-treated and control AAV-Null-treated groups. However, both processes started to resolve in the AAV-*Tbg*-p21-treated group by 48 hours while they were maintained in the AAV-Null-treated mice (Figure S3C, S3D). Serum alanine transferase levels that reflect liver injury were however similar in both groups at both time points (Figure S3E). Although the timing of liver recovery slightly differed between the commonly used APAP model vs APAP/p21 model, the APAP/p21 injury that we established here recapitulated the expected necrosis and progressive recovery. When performed in *Krt19*-Cre^{ERT},*R26*^{LSL}tdTomato mice, APAP/p21 injury induced DR in portal vein areas (Figure 2J), which was significantly milder in the absence of AAV8-*Tbg*-p21 as expected. Two injections of VEGFA mRNA-LNP after APAP administration triggered remarkable BEC-to-hepatocyte conversion (Figure 2K). Numerous large clusters of tdTomato+ hepatocytes were evenly scattered in all liver lobes of VEGFA mRNA-LNP-treated mice, with a % of tdTomato+ areas 20-fold greater than in control LNP-treated mice (Figure 2K). Quantification of tdTomato+ hepatocytes was evaluated using flow cytometry

analysis (Figure 2L) and was further adjusted for lineage tracing efficiency discrepancy (Figure 2L, Figure S3F). Adjusted % tdTomato+ hepatocytes were 5.6-fold greater in VEGFA mRNA-LNP-treated mice compared to control LNP-treated mice (Figure 2L). BEC-derived hepatocytes were identified by co-expression of HNF4A (Figure 2M), and their BEC origin was supported by their proximity to bile ducts (Figure 2M). Interestingly, a few bi-phenotypic tdTomato+ BECs within a bile duct (Figure 2M, yellow arrowheads) were visualized by co-expression of HNF4A as reported[17]. Maturation of tdTomato+ hepatocytes was supported by their ability to store glycogen as efficiently as adjacent tdTomato- hepatocytes (Figure 2N) and to express mature hepatocytic markers found in zone 1/2 or zone 3 such as CPS1 and GS respectively (Figure S3G). Similar to the chronic CDE/p21 injury model, BEC-to-hepatocyte conversion did not occur in APAP-injured mice in the absence of p21-induced senescence in control LNP-treated mice, while small clusters of tdTomato+ hepatocytes were consistently detected in all VEGFA mRNA-LNP-treated mice (Figure S3H). Our data demonstrate the ability of VEGFA mRNA-LNP treatment to trigger BEC-to-hepatocyte conversion that can be further amplified in the presence of hepatocyte senescence in an acute liver injury, suggesting VEGFA mRNA-LNP as an alternative treatment for severe APAP intoxication that would prevent liver failure and, thus, the need for transplantation.

VEGFA mRNA-LNP induces hepatocyte generation from KDR expressing cells in murine acute and chronic liver injury models and improves liver function

To further understand the regenerative role of VEGFA in mice, we identified the liver cell types expressing VEGFR2, also known as KDR, the main functional receptor for VEGFA[57]. As expected, endothelial cells, identified with CD31 expression, are the main liver cells expressing KDR (Figure S4A). Given that BECs have been reported to express KDR in rodent and human diseased livers[38,40], we searched for KDR expression in BECs in the chronic CDE/p21 and acute APAP/p21 mouse models. In both models, we consistently observed expression of KDR in a subpopulation of BECs (Figure 3A, 3B) that was not detected in control uninjured mice treated or not with AAV8-*Tbg*-p21 (Figure S4B), suggesting that KDR marks a subset of BECs that may represent a facultative LPC emerging in response to injury and that could be directly stimulated by VEGFA to generate hepatocytes. To test this hypothesis, we established an inducible *Kdr* lineage tracing line, *Kdr*-2A-Cre^{ERT2}-2A-eYFP,*R26*^{LSL}tdTomato (Figure S4C) allowing cell fate mapping of KDR expressing cells as well as marking KDR expressing cells with YFP. YFP is an accurate tool to track KDR expression as shown with co-staining in endothelial cells (Figure S4C). In control oil-treated mice, some reporter activity was detected in 5.42 ± 1% and 4.68 ± 2% of endothelial cells in females and males, respectively (Figure S4D, S4E, S4F), while leakiness in hepatocytes was almost nonexistent with rare tdTomato+ cells detected in <1:25,000 hepatocytes scanned in all liver lobes from 6 mice (Figure S4G). We further tested the leakiness of this strain during an injury to discriminate between the tdTomato+ hepatocytes derived from KDR+ BECs and the rare tdTomato+ hepatocytes derived from hepatocytes that may have turned on KDR after injury. To do so, we marked all hepatocytes with eGFP following one injection of AAV8-*Tbg*-eGFP prior to injury (Figure S4H), and examined the presence of eGFP-tdTomato+ hepatocytes that originated from KDR+ cells, mostly KDR+ BECs. The acute APAP/p21 injury induced the emergence of large eGFP-

tdTomato+ BEC-derived hepatocyte clusters among areas of eGFP+tdTomato- hepatocytes that were initially eGFP labelled prior to injury (Figure S4I). Only rare eGFP+tdTomato+ hepatocytes were identified that represent hepatocytes in which KDR expression may have been induced after injury. Overall, we were confident to use the *Kdr*-2A-Cre^{ERT2}-2A-eYFP;*R26*^{LSL}tdTomato mice to map the hepatocyte fate of KDR expressing cells. Given the transient expression of KDR on BECs in response to injury, additional tamoxifen injections were included during the period of injury (Figure 3C). The endothelial cell lineage mapping was robust in all mice, as virtually all endothelial cells were tdTomato+ (Figure S4J). We confirmed expression of KDR in a subset of BECs with the *Kdr*-lineage tracing model by the presence of tdTomato+ BEC within biliary ducts (Figure 3D). Analyses of all liver lobes of each mouse revealed an even pattern of tdTomato+ endothelial cells (Figure 3E). Strikingly, some areas were much brighter (Figure 3E, areas within yellow dotted line) and represented tdTomato+ hepatocyte clusters that were significantly larger and more numerous in VEGFA mRNA-LNP-treated mice with a 2.97-fold greater surface area (Figure 3E). Importantly, we confirmed that VEGFA mRNA-LNP treatment significantly reversed steatosis as compared to control-LNP treated mice (Figure 3F) as seen in the CDE/p21-treated *Krt19*-lineage tracing mice. The tdTomato+ clusters were identified as hepatocytes with co-expression of HNF4A and CD26 (Figure 3G). As CD26 is a bile canalicular enzyme that depicts functional polarization of hepatocytes, its expression supports functional maturation of tdTomato+ hepatocytes. As for the *Krt19*-lineage tracing model, extent of DR was similar between the two groups (Figure S4K), most likely due to greater BEC-to-hepatocyte conversion in the VEGFA mRNA-LNP-treated group. The findings were further supported in the acute APAP/p21-induced liver injury (Figure 3H). VEGFA mRNA-LNP significantly promoted emergence of bright tdTomato+ areas (Figure 3I, 6.7-fold increase) identified as hepatocytes with co-staining for HNF4A and CD26 (Figure 3J) as compared to control-LNP-treated mice. Quantification of the KRT7+ BEC areas in both control-LNP- and VEGFA mRNA-LNP-treated mice confirmed again that these numbers were not significantly different (Figure S4L) as found in the CDE/p21 model. These data are reminiscent to observations made in humans following acetaminophen intoxications in which DR decreases as BEC-to-hepatocyte conversion occurs[54]. To capture early events of KDR+ BEC conversion into hepatocytes during APAP/p21 injury, we examined injured *Kdr*-2A-Cre^{ERT2}-2A-eYFP mice (in absence of lineage tracing, Figure S4M) 3 days following APAP administration (Figure 3K). We detected many YFP+ BECs in areas indicative of early regeneration featured by endothelial cell ablation and newly generated hepatocytes with intact DAPI staining (Figure 3K, area delineated with dotted line). The presence of large YFP+ hepatocyte-like cells (Figure 3K, arrows) suggested their differentiation from YFP+KDR+ BECs (Figure 3K, arrowheads).

Overall, findings from complementary *Krt19*- and *Kdr*- lineage tracing models demonstrate the conversion of KDR+ expressing cells, most likely BECs, into hepatocytes which is significantly augmented after VEGFA mRNA-LNP administration.

Liver injury induces emergence of a KDR+ BEC fraction that is molecularly distinct from the KDR- BEC fraction and exhibits VEGF signaling response as well as an epithelial-mesenchymal transition signature

To further characterize the KDR expressing BECs whose emergence is induced with injury, we performed scRNA sequencing analyses on hepatocyte and non-parenchymal cell preparations collected 2 days after APAP overdose in *Krt19*-Cre^{ERT};*R26*^{LSL}tdTomato mice pretreated with AAV-*Tbg*-p21 (Figure 4A). UMAP analyses identified 15 clusters including 2 distinct clusters of BECs, BEC1 and BEC2 (Figure 4B, S5A–C). The BEC1 population represented the mature BECs expressing high levels of the BEC markers (KRT19, KRT7, EpCAM, CFTR, HNF1b, NOTCH pathway)[32,58], while the BEC2 fraction expressed KDR and associated VEGF response-related markers[59], suggesting activation of KDR in these BECs. In line with a progenitor signature, BEC2 expressed markers identified in injury-induced bi-phenotypic progenitor cells or overexpressed in transitioning BECs during the BEC-to-hepatocyte conversion (NES, CD44, KIT, IGFBP5, GATA6, proliferation marker MKi67)[32,58], as well as markers related to epithelial-mesenchymal transition often associated with progenitor feature (VIM, TWIST1, NCAM1, ZEB1, SNAI1, SMO, CDH2)[58] (Figure 4C, 4D). Moreover, GO biological process GSEA analysis of VEGFA/KDR signaling and vasculature development/growth-related signaling showed that they were significantly greater in BEC2 fraction as compared to that in BEC1 fraction. Altogether, these molecular findings support the injury induced-KDR activation in BEC2 population, a unique BEC subset exhibiting molecular progenitor features (Figure 4E, S5D).

VEGFA mRNA-LNP induces BEC differentiation and proliferation of BEC-derived intermediate progenitor cells

To further investigate the mechanisms by which VEGFA mRNA-LNP impacts BEC-to-hepatocyte conversion, we examined the early stages of the conversion process, including BEC proliferation, differentiation into progenitor cells, and their subsequent proliferation. We assessed the effect of VEGFA mRNA-LNP on BEC expansion in CDE/p21 treated C57Bl6 mice that were administered EdU in drinking water for 2 days following a single injection of VEGFA mRNA-LNP or control-LNP (Figure 5A). Mice were sacrificed early to assess the effect of VEGFA in inducing BEC proliferation prior to cell conversion. We found no significant difference between both groups (Figure 5B), results that were also confirmed in the APAP/p21 mice (Figure S5E), indicating that VEGFA mRNA-LNP does not induce BEC proliferation in both injury models (Figure 5B). To track the ability of VEGFA mRNA-LNP to promote BEC differentiation into progenitor cells and the subsequent progenitor proliferation, we used the *Krt19*-Cre^{ERT};*R26*^{LSL}Brainbow line[60] facilitating single cell fate tracing with the 4 reporters. For unknown reason, only cells expressing YFP and GFP and a few expressing RFP were visible on liver sections. We thus simplified our analyses by examining only GFP and YFP reporters that were detected together using an antibody that recognizes both fluorescent proteins. Mice underwent the CDE/p21 injury and were administered a single injection of VEGFA mRNA-LNP instead of two to reduce the number of conversion events that would otherwise affect the tracing of single BECs (Figure 5C). EdU was included in the drinking water for 5 days as soon as VEGFA mRNA-LNP was injected to timely capture the proliferating differentiated BECs. GFP/YFP+ cells within the EpCAM+ BEC population were identified in both VEGFA mRNA-LNP and control-

LNP-treated groups as expected (Figure 5D, yellow arrows for VEGFA-treated group). However, strikingly, a distinct population of GFP/YFP+ EpCAM- clusters were found almost exclusively in the VEGFA-treated group (Figure 5D, white arrows) with number of cells per cluster varying from single cell to more than 6 cells and averaging to 3.5 cells/clusters in the VEGFA mRNA-LNP-treated group as compared to the rare single cells seen in the control-LNP-treated mice (Figure 5E, 5F). Similar GFP/YFP+ EpCAM- clusters were found in the VEGFA mRNA-LNP-treated APAP/p21 injury model (Figure S5F, white arrows). Impressively, by the time of liver collection, most of the GFP/YFP+ cells within the clusters detected in the VEGFA mRNA-LNP-treated CDE/p21 group proliferated (Figure 5G) suggesting their intermediate progenitor stage. The VEGFA mRNA-LNP-induced GFP/YFP+ cells downregulated not only EpCAM but also the other BEC marker KRT7 (Figure 5H, white arrows), while some of them expressed KDR (Figure 5I, yellow arrowheads), and some rare cells expressed low levels of hepatocyte marker HNF4A (Figure 5J, white arrow). The loss of BEC markers and increased proliferation in the GFP/YFP+EpCAM- clusters are reminiscent of the molecular signature of the BEC2 population expressing KDR identified in Figure 4. Altogether, our results demonstrate that VEGFA mRNA-LNP treatment triggers differentiation of BECs into progenitor cells and subsequent proliferation of progenitors. This is a complementary conversion mechanism of VEGFA to the one identified in zebrafish models for which VEGFA promotes differentiation of progenitor cells into hepatocytes.

Identification of KDR expressing BECs with evidence of BEC-to-hepatocyte conversion in human ESLD specimens.

To investigate the clinical relevance of our findings, we sought to identify KDR expressing BECs associated with evidence of BEC-to-hepatocyte conversion in specimens from human explanted ESLD from patients with NASH cirrhosis or alcoholic cirrhosis (n = 5) (Child-Pugh B and C), as well as three normal specimens (Table S1). Histopathological examination confirmed that all five diseased specimens exhibited features of ESLD such as hepatocyte-containing regenerative nodules surrounded with fibrotic septa (Figure S6A, S6B) associated with various degrees of steatosis (Figure S6C) and DR (Figure S6D). As reported in the vast majority of ESLD specimens[61], p21 expression was detected in many hepatocytes in 4 out of 5 specimens (Figure 6A). Numerous KRT7+ cells were also found near the margin of, as well as within, the regenerative nodules (Figure 6B) in all specimens, suggesting the presence of KRT7+ intermediate hepatocyte-like cells derived from KRT7+ BECs as previously speculated in humans[62]. As expected, GS expression in hepatocytes around central vein areas was detected in both diseased and normal specimens (Figure S7A, S7B), however, aberrant GS expression was also found in 4 out of 5 specimens in KRT7+ BECs within DRs and in the adjacent transitioning KRT7+ hepatocytes as well as their neighbors and most likely progeny KRT7-hepatocytes (Figure 6C, S7C) as described[19,23]. GS expression became weaker as hepatocytes were further away from DRs, toward the center of the regenerative nodule (Figure 6C, asterisk). Large GS+ hepatocyte-like cells were often seen budding from strings of smaller KRT7+ BECs (Figure 6C, arrows), an observation that is reminiscent of the hepatocytic buds described two decades ago by Stueck and Wanless[19,21]. Importantly, while KDR expression was not detected in BECs from normal specimens (Figure S7D), numerous KRT7+KDR+ BECs were identified in 2 out of 5 cirrhotic specimens (Figure 7A, specimens HH121 and HH125, arrowheads).

Strikingly, KRT7-KDR+ hepatocyte-like cells (Figure 7A, specimens HH121 and HH125, arrows) were seen budding from strings of KRT7+KDR+ BECs, as observed in mice in the APAP/p21 injury model (*Kdr*-2A-Cre^{ERT2}-2A-eYFP) in which YFP+ hepatocytes were found adjacent to the YFP+KDR+ BECs (Figure 3K, arrows). Expression of cytoplasmic KDR was also detected in a subset of hepatocytes adjacent to KDR+ BECs (Figure 7A, arrows). We further validated KDR expression in purified human hepatocytes from 9 ESLD cirrhotic liver specimens (Child-Pugh score B/C) and compared to normal human liver specimens (Table S1) as previously described[63] at the transcript (Figure 7B, 9 specimens) and protein levels (Figure 7C, 6 specimens). We first validated the hepatocyte identity of the purified cell preparations with the similar levels of *ALB* transcript (Figure S7E) and *HNF4A* transcript representing both promoter P1- and P2- derived *HNF4A* isoforms, including mature and immature variants in the 3 types of specimens including hepatocytes purified from normal and both Child-Pugh score B or C diseased specimens (Figure 7B). As expected from our previous studies, using an antibody that strictly detects the P1-derived adult mature HNF4A variant, protein levels of the mature isoforms were critically downregulated in diseased hepatocytes compared to those in normal hepatocytes (Heps) or normal liver tissue[64–66] (Figure 7C). Importantly, KDR and KRT7 transcript as well as protein levels were upregulated in purified diseased hepatocytes (Figure 7B, 7C) compared to normal human hepatocytes. Of note, diseased hepatocytes expressed the distinct 150 KDa non-glycosylated isoform of KDR (Figure 7C), that was not detected in purified normal hepatocytes nor in normal human liver specimens. These results support the specificity of KDR to diseased hepatocytes as opposed to potential contaminant endothelial cells from the preparations of purified hepatocytes. Indeed, the 230 KDa isoform of KDR was the only variant detected in normal liver tissues that include endothelial cells. The 150 KDa KDR isoform is known to remain in the cytoplasm as an inactive receptor[67] which is consistent with the cytoplasmic staining of KDR observed in specimen sections (Figure 7A, arrows). Although, we cannot conclude about the function of non-glycosylated isoform of KDR in hepatocytes, it serves here as a surrogate lineage tracing mapping the hepatocytic cell fate of KDR expressing BECs. In line with the notion of VEGFA as a therapeutic target for advanced liver diseases, a recent study has shown a significant correlation between high levels of serum VEGF and lower fibrosis score in a NAFLD cohort[68], suggesting a protective effect of VEGFA against progression of the disease. Yet, the study indicates that levels of serum VEGF tend to decrease when NASH develops, offering a potential therapeutic intervention for VEGFA mRNA-LNP to mitigate the liver disease.

Altogether, identification in human ESLD specimens of KDR+ BECs associated with evidence of BEC-to-hepatocyte conversion supported by the presence of KRT7+GS+ hepatocytes and KDR+ hepatocyte-like cells budding from KRT7+GS+ BECs and KRT7+KDR+ BECs, respectively, provides a potential clinical application for VEGFA mRNA-LNP to stimulate BEC-driven liver repair for human liver disease intervention.

Discussion

Hepatocyte-driven repair fails in the face of severe acute injury or years of build-up of chronic liver damage, unveiling the possible clinical benefit of an alternative repair mechanism mediated by BECs. Decades of literature from analyses of human chronic liver

disease specimens identified hepatocytes within regenerative nodules or adjacent to portal vein triads, that harbor BEC marker expression such as KRT7 or EpCAM[16,54,69,70] as well as BECs within the DR turning on a hepatocyte signature with concomitant expression of HNF4A, HNF6 or GS[18–23,70]. Given the clinical context of these human advanced chronic liver disease specimens in which proliferation of senescence gene-expressing hepatocytes is exhausted[49,50,54,56], these observations suggest the BEC origin of the bi-phenotypic hepatocyte-like cells. More recent lineage tracing studies in zebrafish and mouse models of liver injuries have recapitulated the generation of DR and demonstrated BEC-to-hepatocyte conversion when hepatocyte proliferation is compromised[17,26–31]. However, the presence of DR in human advanced chronic liver diseases has been associated with poor prognosis[62], casting a doubt on the BEC ability to promote liver repair and thus questioning their clinical benefit as facultative progenitor cells. Indeed, BECs within DR release profibrogenic factors that may instead aggravate the chronic liver disease features[71,72]. Yet, a recent study showed that aberrant GS positivity in hepatocytes adjacent to portal tracts is significantly associated with regressed cirrhosis in humans[24], suggesting, in contrast, a positive clinical outcome from BEC-derived hepatocytes in resolving human cirrhosis. Altogether, experimental animal model studies combined with analyses of human specimens raise the possibility of leveraging the naturally occurring DR and associated BEC-to-hepatocyte conversion as a therapy if the BEC-driven repair mechanism could be harnessed.

The current challenge for the efficient therapeutic use of BECs is the inability to reliably identify a true progenitor population among them and to, thus, define a druggable pathway that would accelerate their differentiation into functional hepatocytes. The precise identity of BEC liver progenitor cells remains elusive. Some markers such LGR5[73], TROP2[74], FOXL1[75], and ST14[76] have been reported to define BEC progenitors, yet their cell fate mapping during regeneration have not been fully performed or the ability of their progeny to restore liver function fully demonstrated. We and others have identified KDR as a distinct cell surface marker expressed on fetal liver progenitor cells[41], and on developing BECs in human and mice or following injury in mice[38–40]. Here, using complementary mouse and zebrafish liver injury models, we demonstrate that VEGFA, the ligand for KDR, potentializes BEC-driven liver regeneration by promoting BEC-to-hepatocyte conversion with a 5-fold increase on average, and consequently alleviates the liver disease. Mechanistically, our studies in mice reveal that VEGFA significantly induces BEC differentiation into progenitor cells that lose their BEC marker expression and triggers progenitor proliferation, a mechanism that has been recently reported in zebrafish when VEGFR signaling was chemically abrogated as soon as ablation of hepatocytes was initiated[77]. Given that our chemical treatment blocking VEGFR signaling in our zebrafish studies was initiated at a much later time point during hepatocyte ablation, our model showed no BEC differentiation defect, yet reveals at later stages that VEGFR signaling is required for progenitor survival and promotes their conversion into hepatocytes.

Our studies may have significant clinical relevance given the detection of KDR expressing BECs in ESLD liver specimens as well as adjacent KDR expressing hepatocytes, most likely progeny of the KDR expressing BECs. These observations suggest that BEC-to-hepatocyte conversion occurs in humans and is possibly mediated through KDR activation on KDR expressing BECs as our single cell analyses in liver injured mice suggest. Therefore,

if augmented with VEGFA delivered with mRNA-LNP whose safety has been clinically validated[78], BEC-driven liver repair may become an efficient therapy in humans to prevent progression of the chronic liver disease and promote its regression, or to prevent liver failure in acute disease overcoming the necessity for liver transplantation.

Limitations of Study

Our study provides some evidence for the direct role of VEGFA on KDR expressed in BECs to promote BEC-driven repair, a mechanism that was supported in zebrafish by specifically blocking VEGFR signaling in BECs[77]. Yet, it is possible that VEGFA also acts indirectly on other KDR expressing liver cells such as endothelial cells. Specific cell-type KDR knockout mouse model analyses would be instrumental in addressing this point.

STAR★Methods

Resource availability

Lead contact—Further information and requests for resources and reagents should be directed to and will be fulfilled by the lead contact, Valerie Gouon-Evans (valerige@bu.edu).

Materials availability—All unique/stable reagents generated in this study are available from the lead contact without restriction.

Data and code availability—The authors declare that all data supporting the findings of this study are available within the paper and its supplementary information files. Single-cell RNA-seq data have been deposited at GEO at NCBI (https://www.ncbi.nlm.nih.gov/geo/query/acc.cgi?acc=GSE242847) and are publicly available as of the date of publication. Accession numbers are listed in the key resources table. This paper does not report original code. Any additional information required to reanalyze the data reported in this work paper is available from the lead contact upon request.

Experimental model and subject details

In vivo studies—All animal studies were approved by the Boston University IACUC and were consistent with local, state, and federal regulations as applicable. All experiments were done in an age and sex-controlled fashion unless otherwise noted. C57Bl6, *Krt19*-Cre^{ERT} [79], *Kdr*^{tm2Sato}/J, *B6.129P2-Gt(ROSA)26Sor*$^{tm1(CAG-Brainbow2.1)Cle}$*/J* and *R26*^{LSL} tdTomato lines were obtained from Jackson Labs. Animals were housed under standard conditions with a 12-hour day/night cycle, in a pathogen-free environment with access to food and water ad libitum.

For experiments involving study of cell proliferation, mice were administered 0.5mg/ml EdU (5-ethynyl-2'-deoxyuridine) in drinking water for either 2 days or 5 days as indicated. Freshly prepared EdU water was replaced every alternate day where needed.

Generation of *Kdr*-2A-Cre^{ERT2}-2A-eYFP line—The *Kdr* knock-in mouse allele was generated using direct delivery of CRISPR-Cas9 reagents to mouse zygotes. Nucleotide changes in the mouse *Kdr* gene (Ensembl Gene UID ENSMUSG00000062960) were

introduced in the Ensembl Kdr-201 transcript (ENSMUST00000113516.1). The mutant allele inserts the *Kdr*-P2A-CRE^{ERT2}-P2A-YFP. Given that the 2A-Cre^{ERT2}-2A-eYFP cassette was introduced downstream of the last exon of *Kdr* gene, this approach did not affect KDR expression, and homozygous Cre/Cre survive, as opposed to the lethal KDR knockout mice[80].

Gene Editing Design: Analysis of genomic DNA sequence surrounding the target region, using the Benchling (www.benchling.com) guide RNA (gRNA) design tool, identified one gRNA sequence with a suitable target endonuclease site in exon 30. Predicted off-target sites for the gRNA (sgRNA2-ACCTCCTGTTTAAATGGAAG) were identified using the specificity model developed and documented by Hsu and colleagues and embedded in the Benchling gRNA design tool[81]. Design considerations for off-target editing were as follows: higher off-target editing risk was considered when the "Score" is >2.0 with a canonical SpCas9 PAM (NGG), >50.0 with a chromosomally unlinked non-canonical PAM (NAG), or >20.0 with a linked non-canonical PAM yet in an annotated protein coding region. These "Score" thresholds were based on empirical targeted sequencing analysis of 20 different predicted off-target loci in 15 different mouse zygote gene editing experiments.

sgRNAs and plasmid donor DNA repair templates: *Streptococcus pyogenes* Cas9 (SpCas9) mRNA was purchased from Trilink (Product# L-7606, Trilink, USA). sgRNAs were synthesized as described[82]. The sequence of the double stranded DNA donor plasmid, that functions as the DNA repair template, was synthesized by Genscript. Features included asymmetric homology arm lengths of 3kb and 2.2kb, flanking the 2.8kb insertion sequence.

In vitro cell line gRNA evaluation: Using a mouse kidney cell line and a T7 endonuclease cleavage assay, individual gRNA duplexes were evaluated for their ability to direct SpCas9 protein to the target locus and induce a double stranded DNA cleavage event. The immortalized mouse kidney cell line MK4 (a gift from Yueh-Chiang Hu, University of Cincinnati) was infected with a lentivirus construct expressing a SpCas9-P2A-EGFP transgene. Infected cells were selected for high GFP expression using flow cytometry. 200 ng of the sgRNA duplexes were transfected into 50,000 MK4-SpCas9-P2A-EGFP transgenic cells in a 24 well plate using MessengerMax (Product# LMRNA015, ThermoFisher-Invitrogen, USA) according to manufacturer's instructions; 200 ng mCherry mRNA (Product# L-7203, Trilink Biotechnologies, USA) was transfected in a separate well as a control. 24–48 hrs post-transfection, DNA lysates were prepared, and PCR was performed with primers flanking the DNA cleavage target site. PCR products were evaluated on agarose gels.

For evaluating the gRNA activity, the presence of small insertions/deletions (INDELs) in the population of PCR products was detected by denaturation and re-annealing of the PCR product and subsequent treatment with T7 endonuclease (Product# E3321, New England Biolabs, USA). T7 endonuclease cleaves heteroduplex DNA resulting from various INDELs in the population. Unique DNA cleavage products resulting from T7 endonuclease activity were resolved by agarose gel electrophoresis and compared to control transfection PCR products.

Preparation of gene editing reagents for mouse embryo microinjection: The gene editing reagents were prepared for microinjection as described previously[82]. Briefly, 500ng/ul of Cas9 mRNA, 500ng/ul of sgRNA and 500ng/ul donor plasmid were assembled in DNase/RNase free TE buffer, centrifuged and the supernatant collected and delivered for microinjection, all kept on ice or at 4°C.

Zygote isolation, microinjection and embryo transfer: All animal work was approved by the Jackson Laboratory Animal Care and Use Committee and adhered to the standards of the Guide for the Care and Use of Laboratory Animals set forth by the NIH. Fertilized mouse embryos were generated via natural mating and cultured as described previously[82]. C57BL/6J (Stock# 000664, The Jackson Laboratory, USA) donor female mice (3–4 weeks of age) were superovulated by administration of 5 IU of pregnant mare serum gonadotrophin (PMSG) via intraperitoneal (ip) injection (Product# HOR-272 ProSpec, Israel) followed 47 hr later by 5 IU (ip) human chorionic gonadotrophin (hCG) (Product# HOR-250, ProSpec, Israel). Immediately post-administration of hCG, the female was mated 1:1 with a C57BL/6J stud male and 22 hr later checked for the presence of a copulation plug. Female mice displaying a copulation plug were sacrificed, the oviducts excised, and embryos collected. Microinjection was performed as described[82]. In brief, zygotes were microinjected on a Zeiss AxioObserver.D1 using Eppendorf NK2 micromanipulators in conjunction with Narashige IM-5A injectors. Embryos were immediately transferred into B6Qsi5F1 pseudopregnant female mice, a F1 hybrid strain produced by breeding C57BL/6J female mice with the inbred Quackenbush Swiss line 5 (QSi5) mouse strain.

Sequence characterization of Founder and N1 mice: PCR primers flanking the gRNA target site, but outside the repair template homology arms, were used to amplify the region of interest from founder progeny. PCR amplicons were subjected to Sanger sequencing to identify founders with precise desired changes. Founders carrying desired mutations were bred with C57BL/6J mice (Stock #000664, The Jackson Laboratory, USA) to produce N1 progeny. N1 animals were confirmed by the same PCR-Sanger sequence analysis the founder population was subjected to. In contrast to founders, N1 animals are obligate heterozygotes, with one allele derived from an un-manipulated chromosome, enabling deconvolution of the two alleles in the mixed PCR amplicon.

Collection of human liver specimens and hepatocyte isolation—Adult human liver cells were obtained from the Human Synthetic Liver Biology Core at the Pittsburgh Liver Research Center. The Institutional Review Board at the University of Pittsburgh has approved our protocol and given the Not Human Research Determination. The IRB# STUDY20090069. Hepatocytes were isolated using a three-step collagenase digestion technique as previously described[63]. Cell viability was assessed after isolation as previously described using trypan blue exclusion, and only cell preparations with viability > 80% were used for the analysis. Information about the human liver specimens and hepatocytes used in this study can be found in Table S1.

Method details

Acetaminophen (APAP) induced acute injury model—Mice were fasted overnight for a period of 14–15h prior to APAP injections. APAP was administered at a concentration of 20mg/ml, which was freshly dissolved in sterile PBS at 56°C. After complete dissolution, the stock was cooled down to room temperature. A single intraperitoneal injection was administered to male and female mice which received either 300mg/kg or 500mg/kg body weight of APAP, respectively, unless otherwise mentioned. Mice were maintained on normal chow diet and water ad libitum after APAP injections.

CDE diet induced chronic injury model—For inducing the liver injury 7- to 8-week-old male or female mice were given choline-deficient diet (EnvigoTeklad Diets, TD.140207 Choline Deficient Diet with 20% Lard and Irradiated) for one week and then supplemented with 0.10% ethionine in drinking water (Acros Organics,146170100) for another 2 weeks. The mice were either sacrificed at the end of diet or changed to normal diet and drinking water until termination.

Tamoxifen administration and viral infections—Tamoxifen (Sigma-Aldrich) was dissolved in corn oil. For experiments involving *Krt*19-Cre^{ERT2},*R26*^{LSL}tdTomato lines, three individual intraperitoneal tamoxifen injections (20mg/ml) were given at a dose of 4mg/20gm body weight of mice for three alternate days. The AAV8 viral vectors were administered 2 weeks after the last tamoxifen injection. p21 plasmid was packaged into the AAV8.*Tbg* vector by the Penn Vector Core. The null vector, AAV8-control plasmid (AAV8.TBG.PI.Null.bGH, Cat No: AV-8-PV0148) was also obtained from the Penn Vector Core. Viral vectors were diluted in sterile PBS and administered by tail vein or retro-orbital injections with BD Ultra-Fine Insulin Syringes at a viral titer of 5×10^{11} copies in total volume of 100 uL. For experiments involving *Kdr*-2A-Cre^{ERT2}-2A-eYFP,*R26*^{LSL}tdTomato lines, additional 3 tamoxifen injections were given to the mice around the injury as indicated in Figure 4C and Figure 5A. pAAV8.TBG.PI.eGFP.WPRE.bGH (Cat No.: 105535-AAV8) was obtained from Addgene and administered retro-orbitally at two different concentrations namely 1×10^11 gc or 2×10^11 gc. Higher titer was selected for further investigations.

mRNA-LNP formulation and delivery—mRNAs were produced as previously described[83] using T7 RNA polymerase (Megascript, Ambion) on a linearized plasmid encoding codon-optimized[84] vascular endothelial growth factor A (VEGFA) (Table S2) or firefly luciferase (Luc). mRNAs were transcribed to contain 101 nucleotide-long poly(A) tails. One-methylpseudouridine (m1Ψ)-5'-triphosphate (TriLink) instead of UTP was used to generate modified nucleoside-containing mRNA. RNAs were capped using the m7G capping kit with 2'-O-methyltransferase (ScriptCap, CellScript) to obtain cap1. mRNAs were purified by Fast Protein Liquid Chromatography (FPLC) (Akta Purifier, GE Healthcare) or by cellulose purification as described[85,86]. All mRNAs were analyzed by agarose gel electrophoresis and were stored frozen at −20°C. Poly(C) RNA (Sigma) and purified m1Ψ-containing VEGFA and Luc mRNAs were encapsulated in LNP using a self-assembly process in which an aqueous solution of mRNA at pH=4.0 is rapidly mixed with a solution of an ionizable cationic lipid, phosphatidylcholine, cholesterol, and polyethylene glycol-lipid dissolved in ethanol[42]. The ionizable cationic lipid (pKa in the range of 6.0–

6.5, proprietary to Acuitas Therapeutics) and LNP composition are described in the patent application WO 2017/004143. They had a diameter of ~80 nm with a polydispersity index of <0.1 as measured by dynamic light scattering using a Zetasizer Nano ZS (Malvern Instruments Ltd, Malvern, UK) instrument and an encapsulation efficiency of ~95% as determined using a Ribogreen assay. mRNA-LNP formulations were stored at −80°C at a concentration of mRNA of ~1 μg/μl. VEGFA mRNA-LNP as well as control Poly(C) RNA-LNP and Luc mRNA-LNP were delivered intravenously through retro-orbital sinus. Prior to administration, mRNA-LNPs were thawed and diluted on ice in Dulbecco's Phosphate Buffered Saline (PBS). Mice were injected with 50 μl of diluted mRNA-LNP (0.5mg/kg body weight) intravenously by retro-orbital injections using BD Ultra-Fine Insulin Syringes.

Animal tissue harvesting, cryopreservation and serum collection—Mice were sacrificed at their indicated endpoints. The liver was separated into its respective lobes, collected directly in 4% paraformaldehyde (PFA), and kept overnight at 4°C prior to OCT embedding. For cryopreservation, tissues were washed thrice with PBS and dipped in 15% sucrose solution for 15 min and transferred to and kept in 30% sucrose solution till they sunk to the bottom. The tissues were then embedded in OCT. The cryopreserved blocks were stored at −80°C. Livers were sectioned at 5 μm thickness using a cryostat (model CM3050 S; Leica, Wetzlar, Germany) and stored at −20°C until required for subsequent staining. For serum separation, blood was collected immediately after euthanizing the mice and prior to liver extraction and kept at room temperature for 30 min. Serum was separated from blood cells by centrifugation at 2500 × g for 15 min.

Histology, immunohistochemistry and immunofluorescence image analysis—The frozen sections were allowed to defrost and dry at room temperature for 30 min. The slides were dipped in PBS for 10 min and permeabilized using 0.3% triton X in PBS for 10 min. The slides were rinsed thrice in PBS, 10 minutes each, and blocked with 3% normal donkey serum for 30 min. The sections were then incubated overnight at 4°C with appropriate antibody diluted in PBS. Following primary antibody incubations, the slides were washed thrice with PBS, 10 min each, and incubated with the corresponding fluorescent labeled secondary antibodies for 1h at room temperature protected from light. Where needed, after the primary and secondary antibody incubation steps, the slides were processed to detect EdU positive cells using Click-iT™ EdU Imaging KiT according to the manufacturers' instructions. The slides were finally washed, incubated with Dapi for 3–5 min, rinsed, and mounted using FluorSave reagent (EMD Millipore Corp., 345789). ImageJ version 2.3.0/1.53f was used for image analysis as well as quantifications.

Periodic acid–Schiff staining: For staining hepatic glycogen, PAS Staining kit from Sigma Aldrich (395B) was used. Briefly, PFA-fixed, frozen tissue sections were brought to room temperature and hydrated with dH_2O for 10 min. Subsequently, sections were oxidized in 1% periodic acid for 5 min, rinsed in several changes of dH_2O and incubated in Schiff's Reagent for 15 min. After rinsing in dH_2O twice for 5 min each, the tissue was counterstained with hematoxylin for 15 seconds, rinsed, and dehydrated before mounting with permanent mounting solution.

H&E staining: PFA-fixed frozen sections were washed in tap water and dipped for 5 min in hematoxylin (Gill's or Harris), followed by washing in tap water twice for 2 min. Sections were treated with Bluing Reagent (ammonia water) for 10–15 seconds, washed twice and dipped in 100% ethanol. Eosin was applied to sections for 15 sec, thereafter, the slides were washed several times in 100% ethanol, cleared with Histoclear for 5 min, and mounted using permanent mounting media.

Oil Red O staining: Lipid staining was performed on frozen-fixed liver tissue sections using the isopropanol method. Briefly, sections were rinsed with 60% isopropanol and stained with freshly prepared Oil Red O (Sigma) solution for 15 min. Slides were rinsed twice with 60% isopropanol and nuclei were lightly stained using hematoxylin solution. Slides were washed, mounted, and observed under bright-field microscope.

LipidSpot staining: To detect lipid accumulation in liver tissue, another method based on fluorescent detection of lipids was performed using LipidSpot™ Lipid Droplet Stains from Biotium (70065-T). Liver sections were defrosted for 30 minutes at room temperature, followed by an immersion in 1x PBS for 10 minutes at room temperature. Sections were then incubated with a mixture of LipidSpot (1:1000) and DAPI (1:3000) diluted in PBS for 10 minutes at room temperature. The slides were washed twice with PBS for 10 minutes and then mounted with FluorSave mounting media (Calbiochem) and imaged on Nikon Eclipse Ni-E upright fluorescent microscope.

Trichrome staining: Connective Tissue Staining was performed using Trichrome Staining kit (ab150686, Abcam) following the manufacturer's instructions. All materials were equilibrated and prepared at room temperature just prior to use. Frozen sections were hydrated in distilled water prior to staining.

TUNEL assay: Apoptotic and necrotic cells were visualized and quantified using the Invitrogen Click-iT™ Plus TUNEL Assay (Alexa Fluor™ 488 dye). The protocol was adapted for use on frozen-fixed tissue sections by scaling up reagent proportions for larger volumes. Sections were counter-stained with DAPI, mounted, and observed under a fluorescence microscope green channel (Nikon Eclipse Ni-E microscope).

Image Analysis: All immunofluorescence and brightfield images were analyzed using Image J version 2.3.0/1.53f. Stitched images were acquired on Nikon Eclipse Ni-E microscope at 4X objective to capture all the lobes in a plane. For all quantifications, at least three individual representative fields were analyzed per sample unless otherwise mentioned.

Serum ALT Assays—Assays were performed using the Pointe Scientific kits (A7526–450) for testing serum ALT levels, following manufacturers protocol. Briefly, 10 μl of serum diluted in PBS was mixed with supplied reagent mix at 37 °C and readings were measured at 340 nm every 1 min for 5 min using Molecular Devices SpectraMax® i3x Multi-Mode microplate reader.

Human VEGFA (hVEGFA) ELISA with mouse serum—To detect protein expression from hVEGFA-mRNA, serum levels of hVEGFA were analyzed using VEGFA human

ELISA Kit (ab119566, Abcam) following the manufacturer's instructions. Untreated (n=3, females) or injured mice were injected with hVEGFA mRNA-LNP (10μg) through retro-orbital sinus and their serum was collected 5h, 24h, 48h, and 72h post-injection through submandibular bleed. Briefly for the injured group, C57bl6 female mice (n=4) were given single APAP injection (500mg/kg) followed by hVEGFA mRNA-LNP injections 3 days later. For chronic injury group, C57bl6 female mice (n=4) were put on CDD diet for 1 week followed by 2 weeks of supplementation with 0.1% ethionine in drinking water. hVEGFA mRNA-LNP injections was administered 3 days after stopping the diet. Serum samples collected at 5h were diluted 10000-fold, 24h samples were diluted 5000-fold, 48h samples were diluted 10-fold while those collected 72h post-injection were diluted 2-fold. Prior to use all reagents were prepared and equilibrated at room temperature. Samples along with the standards were processed according to the manufacturers protocol and the hVEGFA concentrations were calculated from the standard curve.

Flow cytometry of isolated non-parenchymal cells and hepatocytes—Liver was perfused according to the previously published method[51]. Hepatocyte and non-parenchymal cell fractions were seeded into 100 μl wells and treated with 1 μg/100 μl Fc Block for 10 minutes at room temperature. Wells were then incubated with primary conjugated antibodies for 20 minutes at room temperature. Following antibody incubation, cells were washed and resuspended in FACS buffer. DAPI (1:100, Invitrogen, R37606) was added to the flow tubes 5 min prior to flow run. Cells were run on BD LSR II SORP flow cytometer and data analyzed with FlowJo v10 software. Care was taken to include appropriate compensation controls for each run. UltraComp eBeads (Invitrogen, 01–2222-42) were used for running compensation controls for APC, APC-Cyanine7 and BV605 conjugated antibodies, while DAPI treated non-parenchymal cell (NPC) fractions from a non-tdTomato mouse were used to compensate DAPI channel. Likewise, unlabeled NPCs from tdTomato mouse were used to compensate for tdTomato channel. At least 1,00,000 cells were analyzed for each fraction. Cells in both the hepatocyte fraction or non-parenchymal cell fraction were first gated to eliminate dead cells positive for DAPI. The SSC and FSC parameters were used to eliminate cell debris. The cells were then gated to exclude blood cells positive for Ter119/CD45/CD11b/CD31. The remaining cells in NPC fraction were gated for EpCAM+ and then evaluated for tdTomato positive cells as shown in the gating strategy, while those in hepatocyte fractions were analyzed for tdTomato (Figure S1B).

scRNA sequencing of isolated non-parenchymal cells and hepatocytes—Liver was perfused according to the previously published method[87]. One mouse was perfused at a time making sure that each of the freshly isolated hepatocyte or non-parenchymal cell (NPC) fractions were immediately processed for library preparation using 10X Genomics library preparation kit. Briefly, cell concentration was counted via hemocytometer, in triplicate, then the hepatocyte and NPC fractions were diluted with PBS + 10% FBS to a concentration of 1000 cells/μL, as per 10X Genomics cell prep protocol. Cell concentration after resuspension was confirmed again via hemocytometer. Single cells were captured for sequencing library preparation (3'v3) at the BU scRNA Seq facility using the Chromium Single Cell 3' platform (10X Genomics). Barcoded sequencing libraries were loaded on a NextSeq2000 (Illumina) to obtain a mean sequencing depth ranging from 50K mean reads

per cell. All four samples were sequenced in parallel to minimize batch-to-batch variability. Sequencing files were mapped to the mouse genome reference (mm10) supplemented with eYFP and tdTomato sequence using CellRanger v3.0.2. Seurat v3.2.3[88] was used for downstream analysis and quality control. After inspection of the quality control metrics, cells with 25% of mitochondrial content and <800 detected genes were excluded for downstream analyses. In addition, doublets were also excluded for downstream analysis. We normalized and scaled the unique molecular identifier (UMI) counts using the regularized negative binomial regression (SCTransform)[89]. Following the standard procedure in Seurat's pipeline, we performed linear dimensionality reduction (principal component analysis) and used the top 20 principal components to compute the unsupervised Uniform Manifold Approximation and Projection (UMAP)[90]. For clustering of the cells, we used Louvain algorithm[91] which were computed at a range of resolutions from 1.5 to 0.05 (more to fewer clusters). Populations were annotated using Louvain Clustering at a resolution of 0.05. Cell cycle scores and classifications were done using the Seurat's cell-cycle scoring and regression method[92]. Cluster specific genes were calculated using MAST framework in Seurat wrapper[93]. Gene set enrichment analysis was carried out using fgsea package in R[94] and the database used is Gene Ontology, Biological Process (GO:BP).

Experiments on zebrafish—All zebrafish experiments were performed under the approval of the IACUC at the University of Pittsburgh. Embryos and adult fish were raised and maintained under standard laboratory conditions. We used the following transgenic lines: *Tg(fabp10a:CFP-NTR)*^{s931}, *Tg(Tp1:H2B-mCherry)*^{s939}, *Tg(Tp1:VenusPEST)*^{s940}, *Tg(hs:sflt1)*^{bns80}, *Tg(Tp1:CreERT2)*^{s959}, and *Tg(hs:loxP-mCherry-loxP-hVEGFA)*^{mn32}, and *Tg(hs:hVEGFA-P2A-Venus)*^{pt62}. Their full and official names are listed in resource table.

Generation of the *Tg(hs:hVEGFA-P2A-Venus)* line: Gateway cloning (Thermo Fisher Scientific, Waltham, MA) was used to make the *hs:hVEGFA-P2A-Venus* construct with three entry clones (p5E_the *hsp70l* promoter, pME_*hVEGFA-P2A-Venus*, and p3E_*cryg:CFP-pA*) and a destination vector having two *I-SceI* sites. One nl of the solution containing the final construct (20 ng/μl) and *I-SceI* meganuclease was microinjected into one-cell stage embryos as previously described[95]. The injected larvae expressing CFP in the eyes at 3 dpf were selected and raised to adulthood. Embryos from these adult fish were heat-shocked at 1 dpf to identify founder fish with germline integration. Among several founders, one exhibiting the strongest Venus expression following a heat-shock was selected to establish the line.

Hepatocyte ablation using the Tg(fabp10a:CFP-NTR) line: Hepatocyte ablation was performed by treating Tg(fabp10a:CFP-NTR) larvae with 10 mM Mtz in egg water supplemented with 0.2% DMSO and 0.2 mM 1-phenyl-2-thiourea from 3.5 to 5 dpf for 36 hours, as previously described[31].

SU5416 and ZM323881 hydrochloride treatments: SU5416 and ZM323881 hydrochloride (MedChemExpress, Monmouth Junction, NJ) were used at 1.5 and 1 μM, respectively.

Heat-shock conditions for zebrafish larvae: Both *Tg(hs:sflt1)* and *Tg(hs:loxP-mCherry-loxP-hVEGFA)* larvae were heat-shocked by transferring them into egg water pre-warmed to 38.5°C and keeping them at this temperature for 20 minutes, as previously described[96]. For *Tg(hs:hVEGFA-P2A-Venus)* larvae, 36.5°C was used. **Whole-mount in situ hybridization and immunostaining in zebrafish:** Whole-mount in situ hybridization was performed, as previously described[97], with gc[98] , cp[99] and f5 probes. For f5 probe synthesis, cDNA from 5-dpf larvae was used as a template together with a forward (5′-CCCTCCTGGCATTCCTGTGTC-3′) and a reverse (5′-TAATACGACTCACTATAGGGCATGGTGGGTCTGCAGCTGT-3′) primer pair to amplify f5; its PCR products were used to make in situ probes. [Underlined is T7 primer sequence.] Whole-mount immunostaining was performed, as previously described[100], with mouse anti-Bhmt (1:500; gift from Jinrong Peng at Zhejiang University) and Alexa Fluor 647-conjugated secondary antibodies (1:500; Thermo Fisher Scientific, Waltham, MA).

EdU and TUNEL labeling: EdU labeling was performed according to the protocol outlined in the Click-iT 5-ethynyl-2′-deoxyuridine (EdU) Alexa Fluor 647 Imaging Kit (Thermo Fisher Scientific, Waltham, MA). Larvae were treated with egg water containing 10 mM EdU and 1% DMSO for 6 hours. After the 6-hour EdU treatment, the larvae were harvested for subsequent analysis. Apoptosis assay was performed by TUNEL labeling as described in the protocol of the In Situ Cell Death Detection Kit, TMR red (MilliporeSigma, Burlington, MA).

Quantification of Bhmt+ cell number, Bhmt+ area, and BEC number in the zebrafish liver: For the quantification of Bhmt+ cell number, confocal projection images consisting of 6 optical-section images, with 3-μm interval, were used. Bhmt+ and Tp1:H2B-mCherry+ cells were manually counted; the number of Bhmt/Tp1:H2B-mCherry double-positive cells was divided by the number of Tp1:H2B-mCherry+ cells. For the quantification of Bhmt+ liver area, confocal projection images showing Bhmt and fabp10a:CFP-NTR expression were used. Both Bhmt+ and fabp10a:CFP-NTR+ areas in the liver were calculated by ImageJ and the former area was divided by the latter. For the quantification of BEC number, three single-optical section images, with 6-μm interval, per liver were used. *Tp1:*H2B-mCherry^{strong}/*Tp1:*VenusPEST^{strong} double-positive cells were counted, and their number was divided by liver area.

Image acquisition, processing, and statistical analysis of zebrafish data: Zeiss LSM700 confocal and Leica MZ16 microscopes were used to obtain image data. Confocal stacks were analyzed using the Zen 2009 software. All figures, labels, scale bars and outlines were assembled or drawn using the Adobe Illustrator software. Statistical analyses were performed using the GraphPad Prism software. Differences between groups were tested by unpaired Student's t-tests and considered statistically significant when $P < 0.05$ (*$P < 0.05$, **$P < 0.01$, ***$P < 0.001$, ****$P < 0.0001$).

Human liver tissue staining: Paraffin-embedded liver samples from diseased donors were used as normal liver tissue (n=3). Liver samples from patients with NASH (n=4) and alcoholic cirrhosis (n=1) were fixed overnight in 4% paraformaldehyde (PFA) at 4C. For

cryopreservation, tissues were washed thrice with PBS and dipped in 15% sucrose solution for 15 min and transferred to and kept in 30% sucrose solution till they had sunk to the bottom. The tissues were then embedded in OCT. The cryopreserved blocks were stored at −80°C. Livers were sectioned at 5 μm thickness using a cryostat (model CM3050 S; Leica, Wetzlar, Germany) and stored at −20°C until required for subsequent staining. For all immunofluorescence staining on human liver tissues, antigen-retrieval was performed in Tris-EDTA buffer ph=9 (Vector Labs) for 20 min at 95C followed by conventional permeabilization, blocking and antibody incubation steps as detailed earlier.

Western blot: All samples were incubated with RIPA lysis buffer (Sigma-Aldrich, Saint Louis, MO) containing 1x Halt™ Protease and Phosphatase Inhibitor Cocktail (Thermo Fisher Scientific, Waltham, MA) and incubated for 30 min at 4°C. Samples were centrifuged at 13,000xg for 10 min at 4°C. The supernatant from each sample was then transferred to a new microfuge tube and was used as the whole cell lysate. Protein concentrations were determined by comparison with a known concentration of bovine serum albumin using a Pierce BCA Protein Assay Kit (Thermo Fisher Scientific, Waltham, MA). About 30 μg of lysate were loaded per lane into 10% Mini-PROTEAN TGX gel (BioRad, Hercules, CA). After SDS-PAGE, proteins were transferred onto PVDF membrane (Thermo Fisher Scientific, Waltham, MA). Membranes were incubated with primary antibody solution overnight and then washed. Membranes were incubated for 1 hour in secondary antibody solution and then washed. Target antigens were finally detected using SuperSignal™ West Pico PLUS chemiluminescent substrate (Thermo Fisher Scientific, Waltham, MA). Images were scanned and analyzed using ImageJ software.

Real-time PCR: cDNA samples from human cirrhotic and normal hepatocytes were generated from 2ug of RNA using the RevertAid First Strand cDNA Synthesis Kit (Thermo Scientific, #K1621). Commercially available human liver total RNA (Invitrogen, AM7960) was used as positive control. Information regarding primers used in the study are provided in Table S3. Real-time PCR reaction was performed using SYBR Green PCR Master Mix (Applied Biosystem, 4309155) following manufacturers protocol and run on QuantStudio 6 Flex Real-Time PCR System (Applied Biosystem).

Statistical analyses—All statistical analyses were performed using GraphPad Prism 9. For comparison between two mean values a 2-tailed Student’s t-test was used to calculate statistical significance. For comparing multiple groups to a reference group one-way ANOVA followed by Tukey’s multi-comparison test was performed. Quantitative data are shown as mean ± standard deviation (SD) and are considered statistically significant when $p < 0.05$ (*$p < 0.05$, **$p < 0.01$, ***$p < 0.001$, ****$p < 0.0001$).

Supplementary Material

Refer to Web version on PubMed Central for supplementary material.

Acknowledgments

This work was supported by the NIH R01DK133404 (VG-E and DS), R01DK101426 (DS), and R01AI153064 (NP), DK099257, DK117881, DK119973, TR002383, DK096990, TR003289 and P30DK120531 (Human

Synthetic Liver Biology Core) to AS-G. We are grateful to Anna Belkina of the BUSM Flow Cytometry Core for analytical assistance, supported by NIH Grant 1UL1TR001430, to the Microarray and sequencing Resource (MSR) core facility at BUSM, and Drs. Greg Miller and Marianne James of the CReM, supported by R24HL123828 and U01TR001810. EE and ARS are supported by TL1TR001410 and F31DK127606-01A1. We are grateful to Samuel Morningstar for technical assistance.

Data and code availability

The authors declare that all data supporting the findings of this study are available within the paper and its supplementary information files. The raw and processed scRNA-seq fastq files are available at GEO at NCBI (https://www.ncbi.nlm.nih.gov/geo/query/acc.cgi?acc=GSE242847). Any additional information required to reanalyze the data reported in this paper is available from the lead contact upon request.

Inclusion and Diversity

We support inclusive, diverse, and equitable conduct of research.

References

1. Michalopoulos GK (2017). Hepatostat: Liver regeneration and normal liver tissue maintenance. Hepatology 65, 1384–1392. 10.1002/hep.28988. [PubMed: 27997988]
2. Duncan AW, Dorrell C, and Grompe M (2009). Stem cells and liver regeneration. Gastroenterology137,466–481.S0016–5085(09)00818-X[pii]10.1053/j.gastro.2009.05.044. [PubMed: 19470389]
3. Stanger BZ (2015). Cellular homeostasis and repair in the Mammalian liver. Annu Rev Physiol 77, 179–200. 10.1146/annurev-physiol-021113-170255. [PubMed: 25668020]
4. Rodrigo-Torres D, Affo S, Coll M, Morales-Ibanez O, Millan C, Blaya D, Alvarez-Guaita A, Rentero C, Lozano JJ, Maestro MA, et al. (2014). The biliary epithelium gives rise to liver progenitor cells. Hepatology 60, 1367–1377. 10.1002/hep.27078. [PubMed: 24700364]
5. Shin S, and Kaestner KH (2014). The origin, biology, and therapeutic potential of facultative adult hepatic progenitor cells. Curr Top Dev Biol 107, 269–292. 10.1016/B978-0-12-416022-4.00010-XB978-0-12-416022-4.00010-X [pii]. [PubMed: 24439810]
6. Sato K, Marzioni M, Meng F, Francis H, Glaser S, and Alpini G (2019). Ductular Reaction in Liver Diseases: Pathological Mechanisms and Translational Significances. Hepatology 69, 420–430. 10.1002/hep.30150. [PubMed: 30070383]
7. Boulter L, Lu WY, and Forbes SJ (2013). Differentiation of progenitors in the liver: a matter of local choice. J Clin Invest 123, 1867–1873. 10.1172/JCI6602666026 [pii]. [PubMed: 23635784]
8. Gouw AS, Clouston AD, and Theise ND (2011). Ductular reactions in human liver: diversity at the interface. Hepatology 54, 1853–1863. 10.1002/hep.24613. [PubMed: 21983984]
9. Roskams TA, Theise ND, Balabaud C, Bhagat G, Bhathal PS, Bioulac-Sage P, Brunt EM, Crawford JM, Crosby HA, Desmet V, et al. (2004). Nomenclature of the finer branches of the biliary tree: canals, ductules, and ductular reactions in human livers. Hepatology 39, 1739–1745. 10.1002/hep.20130. [PubMed: 15185318]
10. Roskams T, and Desmet V (1998). Ductular reaction and its diagnostic significance. Semin Diagn Pathol 15, 259–269. [PubMed: 9845427]
11. Popper H, Kent G, and Stein R (1957). Ductular cell reaction in the liver in hepatic injury. J Mt Sinai Hosp N Y 24, 551–556. [PubMed: 13476145]
12. Turanyi E, Dezso K, Csomor J, Schaff Z, Paku S, and Nagy P (2010). Immunohistochemical classification of ductular reactions in human liver. Histopathology 57, 607–614. 10.1111/j.1365-2559.2010.03668.x. [PubMed: 20875072]

13. Lowes KN, Brennan BA, Yeoh GC, and Olynyk JK (1999). Oval cell numbers in human chronic liver diseases are directly related to disease severity. Am J Pathol 154, 537–541. S0002–9440(10)65299–6 [pii]10.1016/S0002-9440(10)65299-6. [PubMed: 10027411]
14. Van Haele M, Snoeck J, and Roskams T (2019). Human Liver Regeneration: An Etiology Dependent Process. Int J Mol Sci 20. 10.3390/ijms20092332.
15. Roskams TA, Libbrecht L, and Desmet VJ (2003). Progenitor cells in diseased human liver. Semin Liver Dis 23, 385–396. 10.1055/s-2004-815564. [PubMed: 14722815]
16. Yoon SM, Gerasimidou D, Kuwahara R, Hytiroglou P, Yoo JE, Park YN, and Theise ND (2011). Epithelial cell adhesion molecule (EpCAM) marks hepatocytes newly derived from stem/progenitor cells in humans. Hepatology 53, 964–973. 10.1002/hep.24122. [PubMed: 21319194]
17. Deng X, Zhang X, Li W, Feng RX, Li L, Yi GR, Zhang XN, Yin C, Yu HY, Zhang JP, et al. (2018). Chronic Liver Injury Induces Conversion of Biliary Epithelial Cells into Hepatocytes. Cell Stem Cell 23, 114–122.e113. 10.1016/j.stem.2018.05.022. [PubMed: 29937200]
18. Haque S, Haruna Y, Saito K, Nalesnik MA, Atillasoy E, Thung SN, and Gerber MA (1996). Identification of bipotential progenitor cells in human liver regeneration. Lab Invest 75, 699–705. [PubMed: 8941215]
19. Stueck AE, and Wanless IR (2015). Hepatocyte buds derived from progenitor cells repopulate regions of parenchymal extinction in human cirrhosis. Hepatology 61, 1696–1707. 10.1002/hep.27706. [PubMed: 25644399]
20. Hytiroglou P, and Theise ND (2018). Regression of human cirrhosis: an update, 18 years after the pioneering article by Wanless et al. Virchows Archiv : an international journal of pathology 473, 15–22. 10.1007/s00428-018-2340-2. [PubMed: 29589101]
21. Wanless IR, Nakashima E, and Sherman M (2000). Regression of human cirrhosis. Morphologic features and the genesis of incomplete septal cirrhosis. Arch Pathol Lab Med 124, 1599–1607. 10.1043/0003-9985(2000)124<1599:Rohc>2.0.Co;2. [PubMed: 11079009]
22. Falkowski O, An HJ, Ianus IA, Chiriboga L, Yee H, West AB, and Theise ND (2003). Regeneration of hepatocyte 'buds' in cirrhosis from intrabiliary stem cells. J Hepatol 39, 357–364. 10.1016/s0168-8278(03)00309-x. [PubMed: 12927921]
23. Fleming KE, and Wanless IR (2013). Glutamine synthetase expression in activated hepatocyte progenitor cells and loss of hepatocellular expression in congestion and cirrhosis. Liver Int 33, 525–534. 10.1111/liv.12099. [PubMed: 23362937]
24. Hadi R, Shin K, Reder N, Alpert L, Koch L, Choi WT, Swanson PE, Hart J, and Westerhoff M (2020). Utility of glutamine synthetase immunohistochemistry in identifying features of regressed cirrhosis. Mod Pathol 33, 448–455. 10.1038/s41379-019-0346-1. [PubMed: 31391527]
25. Lin WR, Lim SN, McDonald SA, Graham T, Wright VL, Peplow CL, Humphries A, Kocher HM, Wright NA, Dhillon AP, and Alison MR (2010). The histogenesis of regenerative nodules in human liver cirrhosis. Hepatology 51, 1017–1026. 10.1002/hep.23483. [PubMed: 20198634]
26. Lu WY, Bird TG, Boulter L, Tsuchiya A, Cole AM, Hay T, Guest RV, Wojtacha D, Man TY, Mackinnon A, et al. (2015). Hepatic progenitor cells of biliary origin with liver repopulation capacity. Nat Cell Biol 17, 971–983. 10.1038/ncb3203ncb3203 [pii]. [PubMed: 26192438]
27. Raven A, Lu WY, Man TY, Ferreira-Gonzalez S, O'Duibhir E, Dwyer BJ, Thomson JP, Meehan RR, Bogorad R, Koteliansky V, et al. (2017). Cholangiocytes act as facultative liver stem cells during impaired hepatocyte regeneration. Nature 547, 350–354. 10.1038/nature23015. [PubMed: 28700576]
28. Russell JO, Lu WY, Okabe H, Abrams M, Oertel M, Poddar M, Singh S, Forbes SJ, and Monga SP (2018). Hepatocyte-specific beta-catenin deletion during severe liver injury provokes cholangiocytes to differentiate into hepatocytes. Hepatology. 10.1002/hep.30270.
29. Manco R, Clerbaux LA, Verhulst S, Bou Nader M, Sempoux C, Ambroise J, Bearzatto B, Gala JL, Horsmans Y, van Grunsven L, et al. (2019). Reactive cholangiocytes differentiate into proliferative hepatocytes with efficient DNA repair in mice with chronic liver injury. J Hepatol 70, 1180–1191. 10.1016/j.jhep.2019.02.003. [PubMed: 30794890]
30. He J, Lu H, Zou Q, and Luo L (2014). Regeneration of liver after extreme hepatocyte loss occurs mainly via biliary transdifferentiation in zebrafish. Gastroenterology 146, 789–800.e788. 10.1053/j.gastro.2013.11.045. [PubMed: 24315993]

31. Choi TY, Ninov N, Stainier DY, and Shin D (2014). Extensive conversion of hepatic biliary epithelial cells to hepatocytes after near total loss of hepatocytes in zebrafish. Gastroenterology 146, 776–788. 10.1053/j.gastro.2013.10.019. [PubMed: 24148620]
32. Oderberg IM, and Goessling W (2023). Biliary epithelial cells are facultative liver stem cells during liver regeneration in adult zebrafish. JCI Insight 8. 10.1172/jci.insight.163929.
33. LeCouter J, Moritz DR, Li B, Phillips GL, Liang XH, Gerber HP, Hillan KJ, and Ferrara N (2003). Angiogenesis-independent endothelial protection of liver: role of VEGFR-1. Science 299, 890–893. 10.1126/science.1079562299/5608/890 [pii]. [PubMed: 12574630]
34. Bockhorn M, Goralski M, Prokofiev D, Dammann P, Grunewald P, Trippler M, Biglarnia A, Kamler M, Niehues EM, Frilling A, et al. (2007). VEGF is important for early liver regeneration after partial hepatectomy. J Surg Res 138, 291–299. S0022–4804(06)00393–3 [pii]10.1016/j.jss.2006.07.027. [PubMed: 17275844]
35. Ding BS, Nolan DJ, Butler JM, James D, Babazadeh AO, Rosenwaks Z, Mittal V, Kobayashi H, Shido K, Lyden D, et al. (2010). Inductive angiocrine signals from sinusoidal endothelium are required for liver regeneration. Nature 468, 310–315. nature09493 [pii]10.1038/nature09493. [PubMed: 21068842]
36. Yang L, Kwon J, Popov Y, Gajdos GB, Ordog T, Brekken RA, Mukhopadhyay D, Schuppan D, Bi Y, Simonetto D, and Shah VH (2014). Vascular endothelial growth factor promotes fibrosis resolution and repair in mice. Gastroenterology 146, 1339–1350.e1331. 10.1053/j.gastro.2014.01.061. [PubMed: 24503129]
37. Oe H, Kaido T, Mori A, Onodera H, and Imamura M (2005). Hepatocyte growth factor as well as vascular endothelial growth factor gene induction effectively promotes liver regeneration after hepatectomy in Solt-Farber rats. Hepatogastroenterology 52, 1393–1397. [PubMed: 16201081]
38. Gaudio E, Barbaro B, Alvaro D, Glaser S, Francis H, Ueno Y, Meininger CJ, Franchitto A, Onori P, Marzioni M, et al. (2006). Vascular endothelial growth factor stimulates rat cholangiocyte proliferation via an autocrine mechanism. Gastroenterology 130, 1270–1282. 10.1053/j.gastro.2005.12.034. [PubMed: 16618418]
39. Dianat N, Dubois-Pot-Schneider H, Steichen C, Desterke C, Leclerc P, Raveux A, Combettes L, Weber A, Corlu A, and Dubart-Kupperschmitt A (2014). Generation of functional cholangiocyte-like cells from human pluripotent stem cells and HepaRG cells. Hepatology 60, 700–714. 10.1002/hep.27165. [PubMed: 24715669]
40. Fabris L, Cadamuro M, Fiorotto R, Roskams T, Spirli C, Melero S, Sonzogni A, Joplin RE, Okolicsanyi L, and Strazzabosco M (2006). Effects of angiogenic factor overexpression by human and rodent cholangiocytes in polycystic liver diseases. Hepatology 43, 1001–1012. 10.1002/hep.21143. [PubMed: 16628643]
41. Goldman O, Han S, Sourrisseau M, Dziedzic N, Hamou W, Corneo B, D'Souza S, Sato T, Kotton DN, Bissig KD, et al. (2013). KDR Identifies a Conserved Human and Murine Hepatic Progenitor and Instructs Early Liver Development. Cell Stem Cell 12, 748–760. 10.1016/j.stem.2013.04.026S1934-5909(13)00193-8 [pii]. [PubMed: 23746980]
42. Pardi N, Tuyishime S, Muramatsu H, Kariko K, Mui BL, Tam YK, Madden TD, Hope MJ, and Weissman D (2015). Expression kinetics of nucleoside-modified mRNA delivered in lipid nanoparticles to mice by various routes. J Control Release 217, 345–351. 10.1016/j.jconrel.2015.08.007S0168-3659(15)30053-5 [pii]. [PubMed: 26264835]
43. Ko S, Choi TY, Russell JO, So J, Monga SPS, and Shin D (2016). Bromodomain and extraterminal (BET) proteins regulate biliary-driven liver regeneration. J Hepatol 64, 316–325. 10.1016/j.jhep.2015.10.017. [PubMed: 26505118]
44. Fong TA, Shawver LK, Sun L, Tang C, App H, Powell TJ, Kim YH, Schreck R, Wang X, Risau W, et al. (1999). SU5416 is a potent and selective inhibitor of the vascular endothelial growth factor receptor (Flk-1/KDR) that inhibits tyrosine kinase catalysis, tumor vascularization, and growth of multiple tumor types. Cancer Res 59, 99–106. [PubMed: 9892193]
45. Sun L, Tran N, Tang F, App H, Hirth P, McMahon G, and Tang C (1998). Synthesis and biological evaluations of 3-substituted indolin-2-ones: a novel class of tyrosine kinase inhibitors that exhibit selectivity toward particular receptor tyrosine kinases. J Med Chem 41, 2588–2603. 10.1021/jm980123i. [PubMed: 9651163]

46. Whittles CE, Pocock TM, Wedge SR, Kendrew J, Hennequin LF, Harper SJ, and Bates DO (2002). ZM323881, a novel inhibitor of vascular endothelial growth factor-receptor-2 tyrosine kinase activity. Microcirculation 9, 513–522. 10.1038/sj.mn.7800164. [PubMed: 12483548]
47. Matsuoka RL, Rossi A, Stone OA, and Stainier DYR (2017). CNS-resident progenitors direct the vascularization of neighboring tissues. Proc Natl Acad Sci U S A 114, 10137–10142. 10.1073/pnas.1619300114. [PubMed: 28855341]
48. Hoeppner LH, Phoenix KN, Clark KJ, Bhattacharya R, Gong X, Sciuto TE, Vohra P, Suresh S, Bhattacharya S, Dvorak AM, et al. (2012). Revealing the role of phospholipase Cβ3 in the regulation of VEGF-induced vascular permeability. Blood 120, 2167–2173. 10.1182/blood-2012-03-417824. [PubMed: 22674805]
49. Marshall A, Rushbrook S, Davies SE, Morris LS, Scott IS, Vowler SL, Coleman N, and Alexander G (2005). Relation between hepatocyte G1 arrest, impaired hepatic regeneration, and fibrosis in chronic hepatitis C virus infection. Gastroenterology 128, 33–42. [PubMed: 15633121]
50. Richardson MM, Jonsson JR, Powell EE, Brunt EM, Neuschwander-Tetri BA, Bhathal PS, Dixon JB, Weltman MD, Tilg H, Moschen AR, et al. (2007). Progressive fibrosis in nonalcoholic steatohepatitis: association with altered regeneration and a ductular reaction. Gastroenterology 133, 80–90. 10.1053/j.gastro.2007.05.012. [PubMed: 17631134]
51. Everton E, Rizvi F, Smith AR, Beattie M, Tam Y, Pardi N, Weissman D, and Gouon-Evans V (2021). Transient yet Robust Expression of Proteins in the Mouse Liver via Intravenous Injection of Lipid Nanoparticle-encapsulated Nucleoside-modified mRNA. Bio Protoc 11, e4184. 10.21769/BioProtoc.4184.
52. Rizvi F, Everton E, Smith AR, Liu H, Osota E, Beattie M, Tam Y, Pardi N, Weissman D, and Gouon-Evans V (2021). Murine liver repair via transient activation of regenerative pathways in hepatocytes using lipid nanoparticle-complexed nucleoside-modified mRNA. Nat Commun 12, 613. 10.1038/s41467-021-20903-3. [PubMed: 33504774]
53. Kofman AV, Morgan G, Kirschenbaum A, Osbeck J, Hussain M, Swenson S, and Theise ND (2005). Dose- and time-dependent oval cell reaction in acetaminophen-induced murine liver injury. Hepatology 41, 1252–1261. 10.1002/hep.20696. [PubMed: 15880565]
54. Katoonizadeh A, Nevens F, Verslype C, Pirenne J, and Roskams T (2006). Liver regeneration in acute severe liver impairment: a clinicopathological correlation study. Liver Int 26, 1225–1233. LIV1377 [pii]10.1111/j.1478-3231.2006.01377.x. [PubMed: 17105588]
55. Yoon E, Babar A, Choudhary M, Kutner M, and Pyrsopoulos N (2016). Acetaminophen-Induced Hepatotoxicity: a Comprehensive Update. Journal of clinical and translational hepatology 4, 131–142. 10.14218/jcth.2015.00052. [PubMed: 27350943]
56. Bird TG, Muller M, Boulter L, Vincent DF, Ridgway RA, Lopez-Guadamillas E, Lu WY, Jamieson T, Govaere O, Campbell AD, et al. (2018). TGFbeta inhibition restores a regenerative response in acute liver injury by suppressing paracrine senescence. Sci Transl Med 10. 10.1126/scitranslmed.aan1230.
57. Holmes K, Roberts OL, Thomas AM, and Cross MJ (2007). Vascular endothelial growth factor receptor-2: structure, function, intracellular signalling and therapeutic inhibition. Cell Signal 19, 2003–2012. S0898–6568(07)00153–2 [pii]10.1016/j.cellsig.2007.05.013. [PubMed: 17658244]
58. Tarlow BD, Pelz C, Naugler WE, Wakefield L, Wilson EM, Finegold MJ, and Grompe M (2014). Bipotential adult liver progenitors are derived from chronically injured mature hepatocytes. Cell Stem Cell 15, 605–618. 10.1016/j.stem.2014.09.008S1934-5909(14)00399-3 [pii]. [PubMed: 25312494]
59. Yang L, Wang WH, Qiu WL, Guo Z, Bi E, and Xu CR (2017). A single-cell transcriptomic analysis reveals precise pathways and regulatory mechanisms underlying hepatoblast differentiation. Hepatology 66, 1387–1401. 10.1002/hep.29353. [PubMed: 28681484]
60. Snippert HJ, van der Flier LG, Sato T, van Es JH, van den Born M, Kroon-Veenboer C, Barker N, Klein AM, van Rheenen J, Simons BD, and Clevers H (2010). Intestinal crypt homeostasis results from neutral competition between symmetrically dividing Lgr5 stem cells. Cell 143, 134–144. 10.1016/j.cell.2010.09.016. [PubMed: 20887898]
61. Pu W, Zhu H, Zhang M, Pikiolek M, Ercan C, Li J, Huang X, Han X, Zhang Z, Lv Z, et al. (2023). Bipotent transitional liver progenitor cells contribute to liver regeneration. Nat Genet 55, 651–664. 10.1038/s41588-023-01335-9. [PubMed: 36914834]

62. Sancho-Bru P, Altamirano J, Rodrigo-Torres D, Coll M, Millán C, José Lozano J, Miquel R, Arroyo V, Caballería J, Ginès P, and Bataller R (2012). Liver progenitor cell markers correlate with liver damage and predict short-term mortality in patients with alcoholic hepatitis. Hepatology 55, 1931–1941. 10.1002/hep.25614. [PubMed: 22278680]

63. Gramignoli R, Green ML, Tahan V, Dorko K, Skvorak KJ, Marongiu F, Zao W, Venkataramanan R, Ellis EC, Geller D, et al. (2012). Development and application of purified tissue dissociation enzyme mixtures for human hepatocyte isolation. Cell Transplant 21, 1245–1260. 10.3727/096368911x600939. [PubMed: 22080793]

64. Aguila HL, Akashi K, Domen J, Gandy KL, Lagasse E, Mebius RE, Morrison SJ, Shizuru J, Strober S, Uchida N, et al. (1997). From stem cells to lymphocytes: biology and transplantation. Immunol Rev 157, 13–40. [PubMed: 9255619]

65. Nishikawa T, Bell A, Brooks JM, Setoyama K, Melis M, Han B, Fukumitsu K, Handa K, Tian J, Kaestner KH, et al. (2015). Resetting the transcription factor network reverses terminal chronic hepatic failure. J Clin Invest 125, 1533–1544. 10.1172/jci73137 [PubMed: 25774505]

66. Guzman-Lepe J, Cervantes-Alvarez E, Collin de l'Hortet A, Wang Y, Mars WM, Oda Y, Bekki Y, Shimokawa M, Wang H, Yoshizumi T, et al. (2018). Liver-enriched transcription factor expression relates to chronic hepatic failure in humans. Hepatology communications 2, 582–594. 10.1002/hep4.1172. [PubMed: 29761173]

67. Takahashi T, and Shibuya M (1997). The 230 kDa mature form of KDR/Flk-1 (VEGF receptor-2) activates the PLC-gamma pathway and partially induces mitotic signals in NIH3T3 fibroblasts. Oncogene 14, 2079–2089. 10.1038/sj.onc.1201047 [PubMed: 9160888]

68. Papageorgiou MV, Hadziyannis E, Tiniakos D, Georgiou A, Margariti A, Kostas A, and Papatheodoridis GV (2017). Serum levels of vascular endothelial growth factor in non-alcoholic fatty liver disease. Ann Gastroenterol 30, 209–216. 10.20524/aog.2016.0107. [PubMed: 28243042]

69. Vandersteenhoven AM, Burchette J, and Michalopoulos G (1990). Characterization of ductular hepatocytes in end-stage cirrhosis. Arch Pathol Lab Med 114, 403–406. [PubMed: 2322100]

70. Limaye PB, Alarcón G, Walls AL, Nalesnik MA, Michalopoulos GK, Demetris AJ, and Ochoa ER (2008). Expression of specific hepatocyte and cholangiocyte transcription factors in human liver disease and embryonic development. Lab Invest 88, 865–872. 10.1038/labinvest.2008.56. [PubMed: 18574450]

71. Kaur S, Siddiqui H, and Bhat MH (2015). Hepatic Progenitor Cells in Action: Liver Regeneration or Fibrosis? Am J Pathol 185, 2342–2350. 10.1016/j.ajpath.2015.06.004. [PubMed: 26255773]

72. Glaser SS, Gaudio E, Miller T, Alvaro D, and Alpini G (2009). Cholangiocyte proliferation and liver fibrosis. Expert Rev Mol Med 11, e7. 10.1017/s1462399409000994. [PubMed: 19239726]

73. Huch M, Dorrell C, Boj SF, van Es JH, Li VS, van de Wetering M, Sato T, Hamer K, Sasaki N, Finegold MJ, et al. (2013). In vitro expansion of single Lgr5(+) liver stem cells induced by Wnt-driven regeneration. Nature. 10.1038/nature11826nature11826 [pii].

74. Okabe M, Tsukahara Y, Tanaka M, Suzuki K, Saito S, Kamiya Y, Tsujimura T, Nakamura K, and Miyajima A (2009). Potential hepatic stem cells reside in EpCAM+ cells of normal and injured mouse liver. Development 136, 1951–1960. 136/11/1951 [pii]10.1242/dev.031369. [PubMed: 19429791]

75. Shin S, Walton G, Aoki R, Brondell K, Schug J, Fox A, Smirnova O, Dorrell C, Erker L, Chu AS, et al. (2011). Foxl1-Cre-marked adult hepatic progenitors have clonogenic and bilineage differentiation potential. Genes Dev 25, 1185–1192. 10.1101/gad.202781125/11/1185 [pii]. Journ [PubMed: 21632825]

76. Li B, Dorrell C, Canaday PS, Pelz C, Haft A, Finegold M, and Grompe M (2017). Adult Mouse Liver Contains Two Distinct Populations of Cholangiocytes. Stem Cell Reports 9, 478–489. 10.1016/j.stemcr.2017.06.003 [PubMed: 28689996]

77. Cai P, Ni R, Lv M, Liu H, Zhao J, He J, and Luo L (2023). VEGF signaling governs the initiation of biliary-mediated liver regeneration through the PI3K-mTORC1 axis. Cell Rep 42, 113028. 10.1016/j.celrep.2023.113028. [PubMed: 37632748]

78. Weissman D (2015). mRNA transcript therapy. Expert Rev Vaccines 14, 265–281. 10.1586/14760584.2015.973859. [PubMed: 25359562]

79. Means AL, Xu Y, Zhao A, Ray KC, and Gu G (2008). A CK19(CreERT) knockin mouse line allows for conditional DNA recombination in epithelial cells in multiple endodermal organs. Genesis 46, 318–323. 10.1002/dvg.20397. [PubMed: 18543299]
80. Shalaby F, Rossant J, Yamaguchi TP, Gertsenstein M, Wu XF, Breitman ML, and Schuh AC (1995). Failure of blood-island formation and vasculogenesis in Flk-1-deficient mice. Nature 376, 62–66. 10.1038/376062a0. [PubMed: 7596435]
81. Hsu PD, Scott DA, Weinstein JA, Ran FA, Konermann S, Agarwala V, Li Y, Fine EJ, Wu X, Shalem O, et al. (2013). DNA targeting specificity of RNA-guided Cas9 nucleases. Nat Biotechnol 31, 827–832. 10.1038/nbt.2647. [PubMed: 23873081]
82. Qin W, Dion SL, Kutny PM, Zhang Y, Cheng AW, Jillette NL, Malhotra A, Geurts AM, Chen YG, and Wang H (2015). Efficient CRISPR/Cas9-Mediated Genome Editing in Mice by Zygote Electroporation of Nuclease. Genetics 200, 423–430. 10.1534/genetics.115.176594. [PubMed: 25819794]
83. Pardi N, Muramatsu H, Weissman D, and Kariko K (2013). In vitro transcription of long RNA containing modified nucleosides. Methods Mol Biol 969, 29–42. 10.1007/978-1-62703-260-5_2. [PubMed: 23296925]
84. Thess A, Grund S, Mui BL, Hope MJ, Baumhof P, Fotin-Mleczek M, and Schlake T (2015). Sequence-engineered mRNA Without Chemical Nucleoside Modifications Enables an Effective Protein Therapy in Large Animals. Mol Ther 23, 1456–1464. 10.1038/mt.2015.103. [PubMed: 26050989]
85. Weissman D, Pardi N, Muramatsu H, and Kariko K (2013). HPLC purification of in vitro transcribed long RNA. Methods Mol Biol 969, 43–54. 10.1007/978-1-62703-260-5_3. [PubMed: 23296926]
86. Baiersdörfer M, Boros G, Muramatsu H, Mahiny A, Vlatkovic I, Sahin U, and Karikó K (2019). A Facile Method for the Removal of dsRNA Contaminant from In Vitro-Transcribed mRNA. Molecular therapy. Nucleic acids 15, 26–35. 10.1016/j.omtn.2019.02.018. [PubMed: 30933724]
87. Everton E, Del Rio-Moreno M, Villacorta-Martin C, Singh Bawa P, Lindstrom-Vautrin J, Muramatsu H, Rizvi F, Smith AR, Tam Y, Pardi N, et al. (2023). Growth Hormone Accelerates Recovery From Acetaminophen-Induced Murine Liver Injury. bioRxiv. 10.1101/2023.04.17.537197.
88. Stuart T, Butler A, Hoffman P, Hafemeister C, Papalexi E, Mauck WM 3rd, Hao Y, Stoeckius M, Smibert P, and Satija R (2019). Comprehensive Integration of Single-Cell Data. Cell 177, 1888–1902.e1821. 10.1016/j.cell.2019.05.031. [PubMed: 31178118]
89. Hafemeister C, and Satija R (2019). Normalization and variance stabilization of single-cell RNA-seq data using regularized negative binomial regression. Genome Biol 20, 296. 10.1186/s13059-019-1874-1. [PubMed: 31870423]
90. McInnes L, Healy J, Melville J UMAP: Uniform Manifold Approximation and Projection for Dimension Reduction. https://arxiv.org/pdf/1802.03426.pdf.
91. Blondel VD, Guillaume J-L, Lambiotte R, Lefebvre E Fast unfolding of communities in large networks. J Stat Mech. 2008;2008(10):P10008.
92. Tirosh I, Izar B, Prakadan SM, Wadsworth MH 2nd, Treacy D, Trombetta JJ, Rotem A, Rodman C, Lian C, Murphy G, et al. (2016). Dissecting the multicellular ecosystem of metastatic melanoma by single-cell RNA-seq. Science 352, 189–196. 10.1126/science.aad0501. [PubMed: 27124452]
93. Finak G, McDavid A, Yajima M, Deng J, Gersuk V, Shalek AK, Slichter CK, Miller HW, McElrath MJ, Prlic M, et al. (2015). MAST: a flexible statistical framework for assessing transcriptional changes and characterizing heterogeneity in single-cell RNA sequencing data. Genome Biol 16, 278. 10.1186/s13059-015-0844-5. [PubMed: 26653891]
94. Korotkevich G, Sukhov V, Sergushichev A Fast gene set enrichment analysis. bioRxiv (2019).
95. Grabher C, Joly JS, and Wittbrodt J (2004). Highly efficient zebrafish transgenesis mediated by the meganuclease I-SceI. Methods Cell Biol 77, 381–401. 10.1016/s0091-679x(04)77021-1. [PubMed: 15602923]
96. Shin D, Shin CH, Tucker J, Ober EA, Rentzsch F, Poss KD, Hammerschmidt M, Mullins MC, and Stainier DY (2007). Bmp and Fgf signaling are essential for liver specification in zebrafish. Development 134, 2041–2050. [PubMed: 17507405]

97. Alexander J, Stainier DY, and Yelon D (1998). Screening mosaic F1 females for mutations affecting zebrafish heart induction and patterning. Dev Genet 22, 288–299. 10.1002/(sici)1520-6408(1998)22:3<288::Aid-dvg10>3.0.Co;2-2. [PubMed: 9621435]

98. Noël ES, Reis MD, Arain Z, and Ober EA (2010). Analysis of the Albumin/alpha-Fetoprotein/Afamin/Group specific component gene family in the context of zebrafish liver differentiation. Gene Expr Patterns 10, 237–243. 10.1016/j.gep.2010.05.002. [PubMed: 20471496]

99. Korzh S, Emelyanov A, and Korzh V (2001). Developmental analysis of ceruloplasmin gene and liver formation in zebrafish. Mech Dev 103, 137–139. [PubMed: 11335121]

100. Choi TY, Khaliq M, Ko S, So J, and Shin D (2015). Hepatocyte-specific ablation in zebrafish to study biliary-driven liver regeneration. J Vis Exp, e52785. 10.3791/52785. [PubMed: 26065829]

Highlights

1. VEGFA mRNA-LNP in mice triggers conversion of BECs into functional hepatocytes
2. VEGFA mRNA-LNP reverts steatosis and fibrosis in mice
3. VEGFA mRNA-LNP in mice induces differentiation of BECs into proliferating LPCs
4. Presence of KDR+ BECs near KDR+ hepatocytes in human ESLD suggests their BEC origin

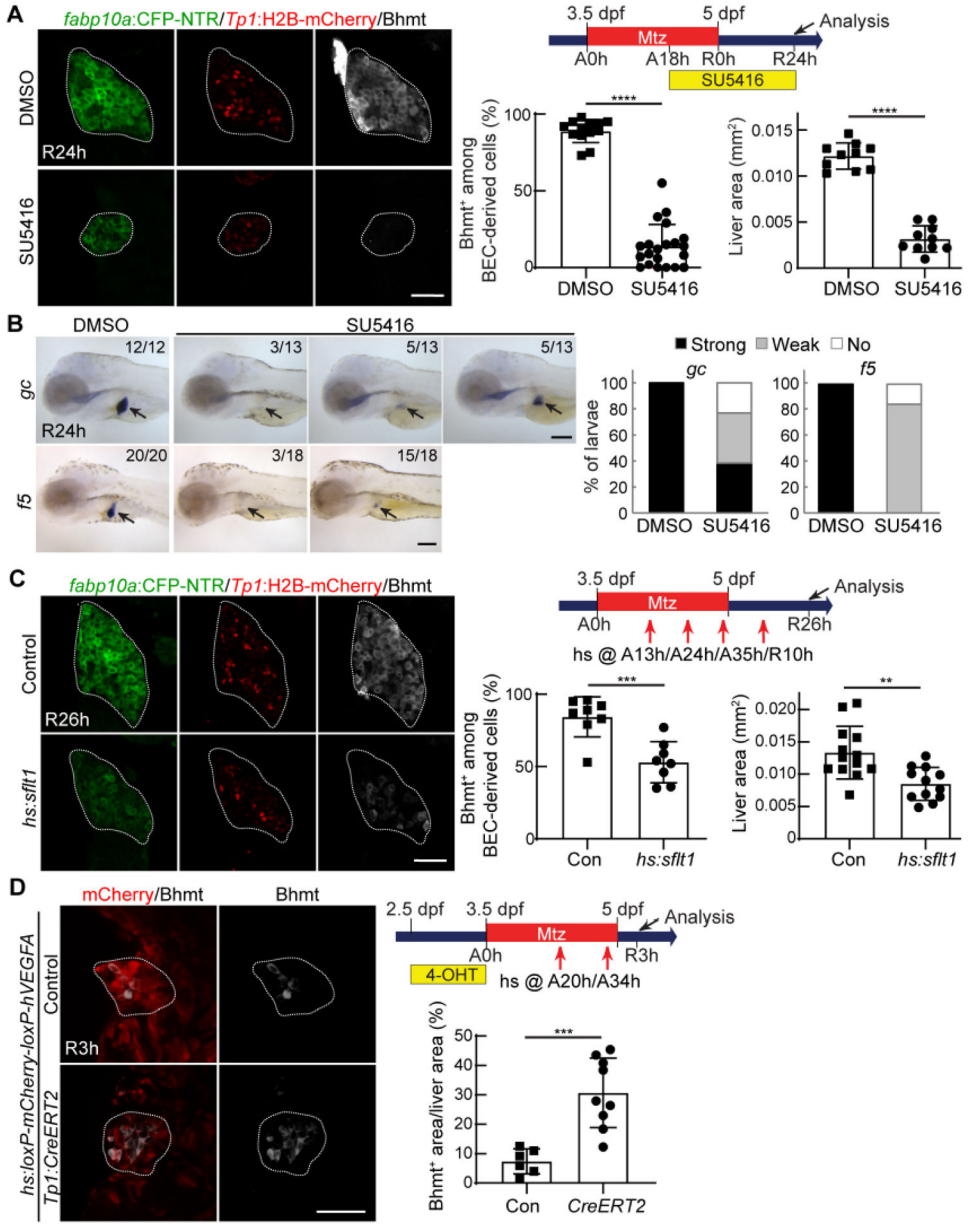

Figure 1. VEGFR signaling regulates BEC-driven liver regeneration in zebrafish.

(A) Single-optical section images showing the expression of Bhmt (gray), *Tp1:*H2B-mCherry (red), and *fabp10a:*CFP-NTR (green) in regenerating livers (dotted lines) at R24h. Scheme illustrates the periods of Mtz and SU5416 treatments and analysis stage. Quantification of the percentage of hepatocytes (Bhmt^{+}) among BEC-derived cells (H2B-mCherry^{+}) and of liver size.

(B) Whole-mount in situ hybridization images showing *gc* and *f5* expression (arrows) in regenerating livers at R24h. Numbers in the upper-right corner indicate the proportion of larvae exhibiting the phenotype shown. Based on the levels of hepatic *gc* and *f5* expression, larvae were divided into three groups: no, weak, and strong.

(C) Single-optical section images showing the expression of *Tp1:*H2B-mCherry, *fabp10a:*CFP-NTR, and Bhmt in regenerating livers (dashed lines) at R26h. To overexpress sFlt1, *Tg(hs:sflt1)* larvae were heat-shocked four times at A13h, A24h, A35h, and R10h. Quantification of the percentage of $Bhmt^+$ among BEC-derived cells and of liver size. **(D)** Maximum projection images showing the expression of *hs:loxP*-mCherry-*loxP* and Bhmt in regenerating livers (dashed lines) at R3h. The *Tg(Tp1:CreERT2)* and *Tg(hs:loxP-mCherry-loxP-hVEGFA)* lines were used to express hVEGFA in a subset of BEC-derived cells during regeneration. Larvae were treated with 10 μM 4-OHT from 2.5 to 3.5 dpf for 24 hours, heat-shocked twice at A20h and A34h, and harvested at R3h. Quantification of the percentage of $Bhmt^+$ area in the liver. Data are presented as mean ± SEM. Unpaired two-tailed t-test, **p<0.01, ***p<0.001, and ****p<0.0001. Scale bars: Scale bars: 50μm (A,C,D), 100μm (B). See also Figure S1.

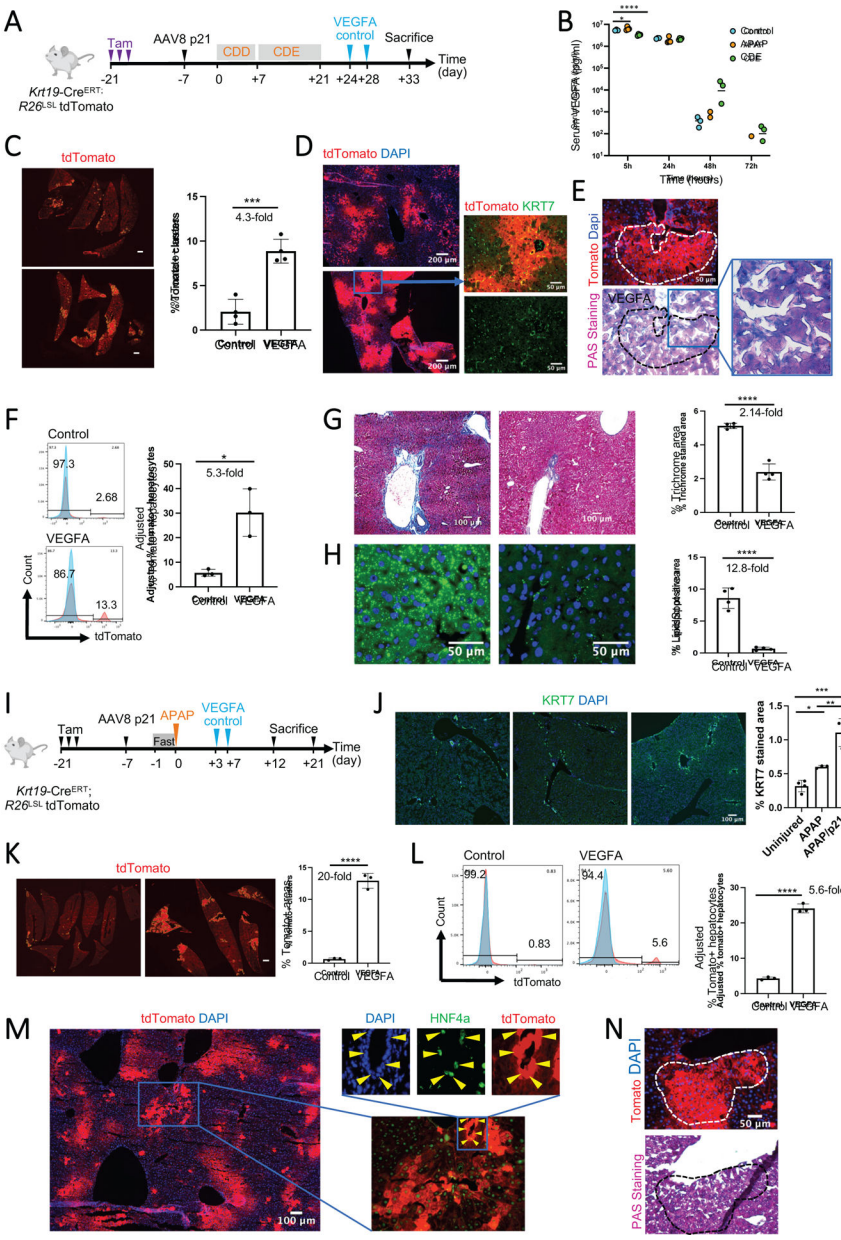

Figure 2. VEGFA mRNA-LNP induces BEC-to-hepatocyte conversion and promotes liver repair in chronic CDE/p21 and acute APAP/p21 liver injury models in *Krt19*-Cre^{ERT},*R26*^{LSL}tdTomato mice.

(**A)** Schematic depicting CDE/p21 injury model in female mice.

(B) Human-specific VEGFA ELISA from sera of uninjured control (n=3), or mice injured with APAP (n=4) or CDE (n=4).

(C) Stitched images of tdTomato+ clusters (outlined yellow) in livers from CDE/p21 injured mice. Quantification of tdTomato+ areas in both groups.

(D) tdTomato+ (red) and KRT7+ (green) cells in the CDE/p21 model. Close-up images of tdTomato+ hepatocytes (arrowheads) adjacent to tdTomato+KRT7+ BECs (arrows) in VEGFA mRNA-LNP-treated mice. * Represents tdTomato+ BECs.

(E) tdTomato and PAS staining on serial sections of liver tissue showing glycogen storage in tdTomato+ hepatocytes in CDE/p21 model.

(F) Representative histograms from flow cytometry of hepatocyte fractions from female *Krt19*-Cre^{ERT},*R26*^{LSL}tdTomato mice treated as shown in Figure 2A. Red histograms represent % tdTomato+ populations within the hepatocyte fractions. Blue histograms represent hepatocytes from a control non-tdTomato background. Calculation of % tdTomato+ hepatocytes by extrapolating the lineage tracing efficiency as 100% across all mice in CDE/p21 model.

(G) Brightfield images and quantification of % trichrome-positive areas from three different fields in each mouse (n=4 mice per treatment) in CDE/p21 model.

(H) Images of LipidSpot staining showing lipids (green) in hepatocytes and quantification of % LipidSpot-stained areas from three different fields in each mouse (n=4 mice per treatment) in CDE/p21 model.

(I) Schematic depicting APAP/p21 injury model in female mice.

(J) Immunofluorescence images and quantification of KRT7+ BECs in APAP or APAP/p21 models 12 days after APAP.

(K) Stitched immunofluorescence images of tdTomato+ areas (outlined in yellow) in APAP/p21 model and quantification of tdTomato+ areas.

(L) Representative histograms from flow cytometry of hepatocyte fractions isolated 21 days after APAP from male *Krt19*-Cre^{ERT},*R26*^{LSL}tdTomato mice treated as shown in Figure 2I with 300mg/kg APAP. Red histograms represent % tdTomato+ populations within the hepatocyte fractions, and blue histograms, the hepatocytes from a control non-tdTomato background. Calculation of % tdTomato+ hepatocytes by extrapolating the lineage tracing efficiency as 100% across all mice.

(M) Immunofluorescence images of tdTomato+ hepatocyte (arrows) in APAP/p21 model costained with HNF4A (green) 21 days after injury. Close-up images of HNF4A+ cells within a tdTomato+ biliary duct.

(N) tdTomato and PAS staining on serial sections of liver demonstrating glycogen storage in tdTomato+ hepatocytes in APAP/p21 model 21 days after injury.

Numerical data are presented as mean ± s.d. Two-tailed Student’s t-test, *p< 0.05, **p< 0.01, ***p < 0.001, ****p<0.0001. See also Figure S2 and S3.

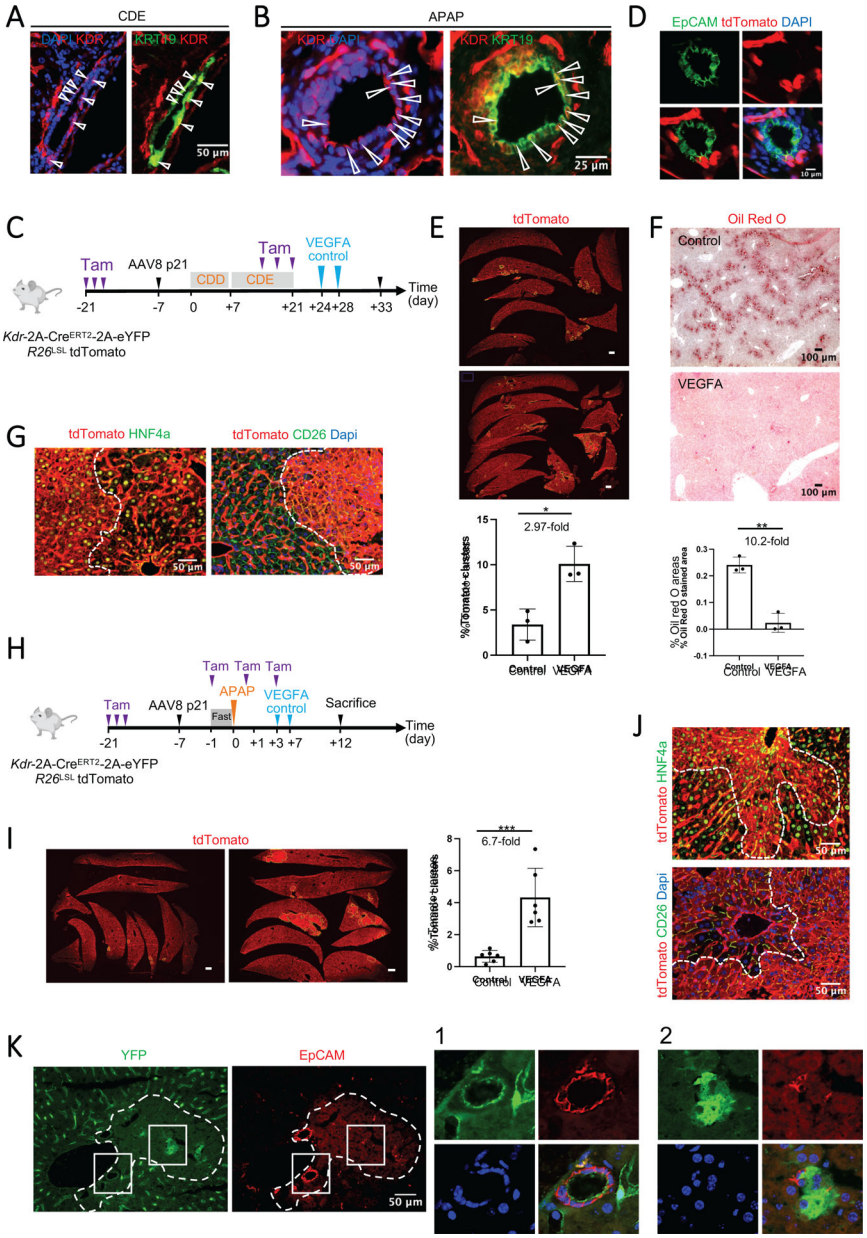

Figure 3. VEGFA mRNA-LNP induces BEC-to-hepatocyte conversion and promotes liver repair in chronic CDE/p21 and acute APAP/p21 liver injury models in *Kdr*-2A-Cre^{ERT2}-2Ae-YFP mice.

(A, B) Expression of KDR (red) in BECs (green) depicted by arrowheads 3 days after injury in female mice in CDE/p21 (A) and APAP/p21 (B) models. **(C)** Schematic depicting the CDE/p21 model.

(D) Close-up images of a bile duct showing tdTomato+ EpCAM+ BECs in CDE/p21 injury model.

(E) Stitched immunofluorescence images of tdTomato+ areas (outlined yellow) in CDE/p21 injury model. Quantification of the tdTomato+ areas in both groups.

(F) Representative brightfield images of Oil Red O-stained liver showing lipids in CDE/p21 injury model. Quantification of the % Oil Red O-stained areas averaged from three different fields in each mouse (n=3 mice per group).

(G) Immunofluorescence images of tdTomato+ hepatocytes costained with HNF4A or CD26 (outlined and identified with *) in CDE/p21 injury model.
(H) Schematic of the APAP/p21 injury model with 300 mg/kg for males (n=6) or 500 mg/kg for females (n=6).
(I) Stitched immunofluorescence images of tdTomato+ areas (outlined yellow) and quantification of tdTomato+ areas in APAP/p21 injury model.
(J) Immunofluorescence images of tdTomato+ hepatocytes (outlined and identified with *) in APAP/p21 injury model costained with HNF4A (green) or CD26 (green).
(K) Immunofluorescence images of YFP+ liver cells in *Kdr*-2A-Cre^{ERT2}-2A-eYFP mice 3 days after APAP (400 mg/kg for male or 500 mg/kg for female). Close-ups show BECs co-expressing YFP (green) and EpCAM (red) (arrowheads) and large intermediate hepatocyte-like cells expressing YFP (green) (arrows).
Numerical data are presented as mean ± s.d. Two-tailed Student's t-test, *p< 0.05, **p< 0.01, ***p < 0.001. See also Figure S4.

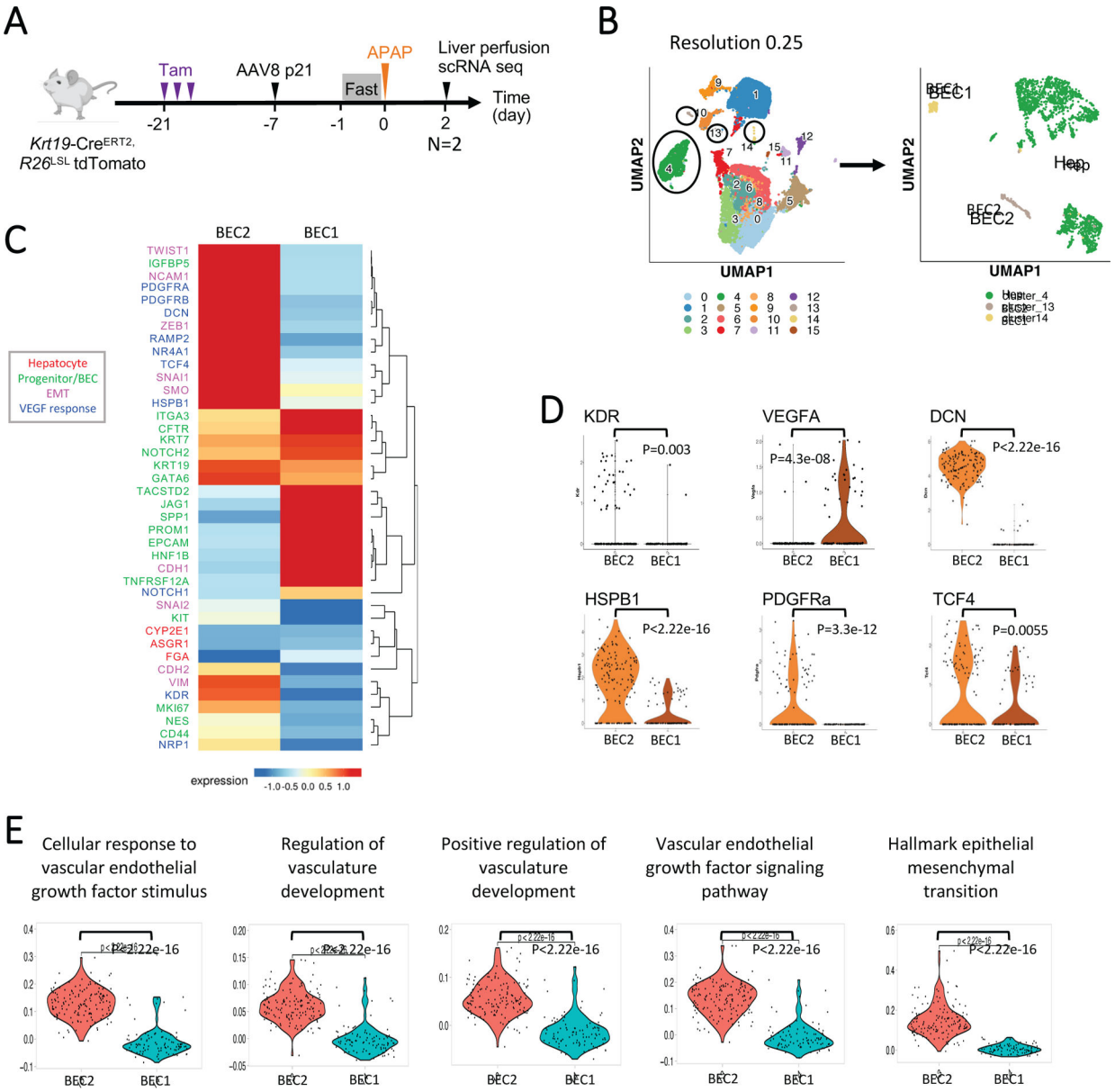

Figure 4. KDR+ BEC fraction after liver injury is molecularly distinct from the KDR- BEC fraction and exhibits VEGF signaling response as well as an epithelial-mesenchymal transition signature.

(A) Experimental design for scRNA seq experiment. In total 2 hepatocyte and 2 NPC fractions were analyzed from 2 mice.

(B) UMAP of the scRNA seq data at the Louvain resolution 0.25. UMAP on the right is obtained after re-clustering of cluster 4 (Hep), cluster 13 (BEC2) and cluster 14 (BEC1) from the UMAP on the left.

(C) Heatmap of few key genes related to hepatocytes, progenitor/BEC, EMT and VEGF response in BEC1 and BEC2 clusters.

(D) Violin plots for selected genes in BEC1 and BEC2 populations.

(E) Violin plots for GO biological process GSEA analysis using differential genes expressed between BEC2 and BEC1 populations.

P value calculated with paired t-test. See also Figure S5.

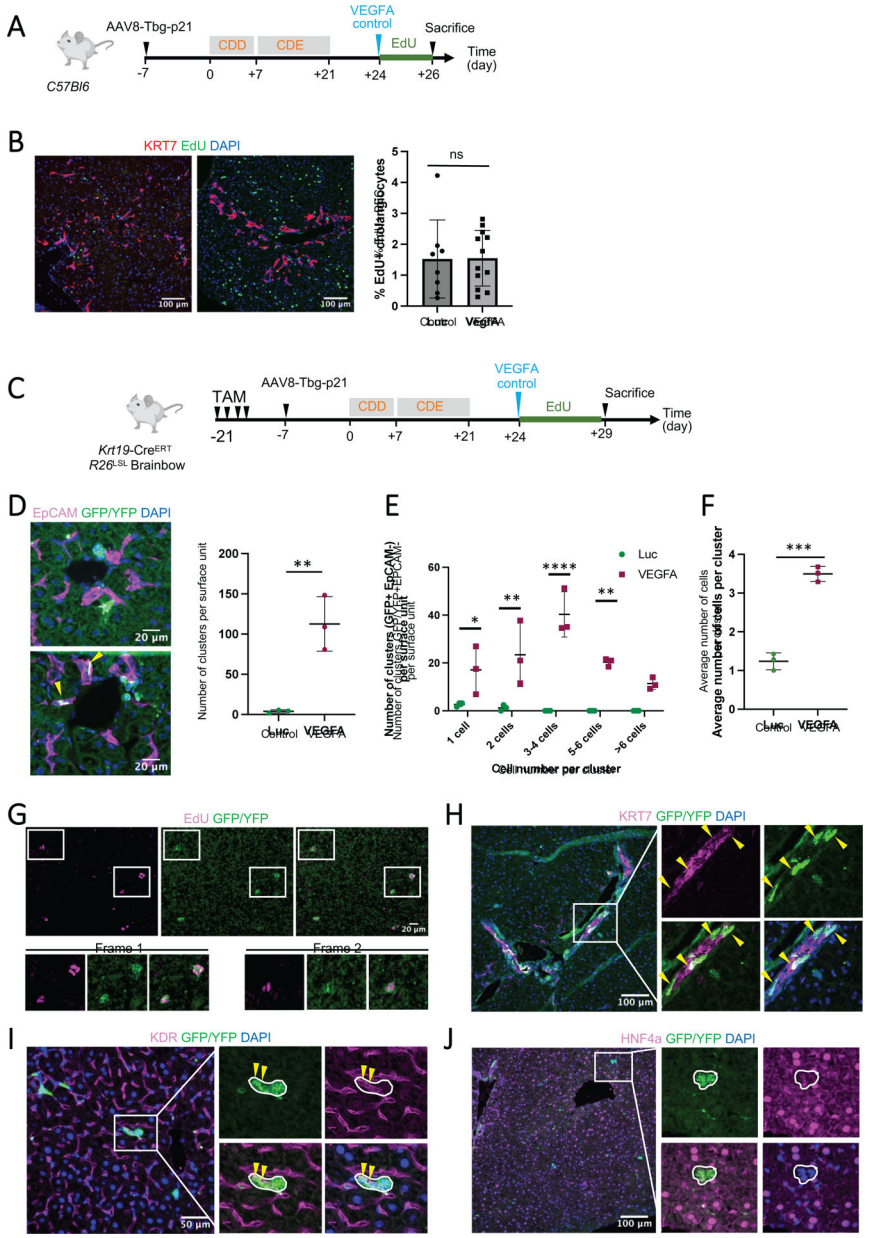

Figure 5. VEGFA mRNA-LNP increases the numbers of BEC-derived progenitor cells in chronically injured mouse livers.

(A) Schematic of the CDE/p21 injury model for (B).

(B) Immunofluorescence images of proliferative EdU+ cells and KRT7+ BECs. Quantitation of KRT7+EdU+ BECs using 3 image fields per mice.

(C) Schematic of the CDE/p21 injury model for (C-H).

(D) Immunofluorescence images of GFP/YFP+ cells and EpCAM+ BECs. Quantitation of GFP/YFP+EpCAM- clusters in both groups (n=3 mice per group). All liver lobes in control Luc group were analyzed, while only 2 lobes per mice were in VEGFA group.

(E) Distribution of GFP/YFP+EpCAM- clusters based on numbers of cells per cluster.

(F) Averaged numbers of GFP/YFP+EpCAM- cells per cluster.

(G) Immunofluorescence images of proliferative GFP/YFP+EdU+ cells in VEGFA mRNA-LNP-treated mice in CDE/p21 injury model.
(H) Immunofluorescence images of GFP/YFP+ cells and KRT7+ BECs. Yellow arrowheads denote GFP/YFP+KRT7+ cells and white arrows GFP/YFP+KRT7- cells.
(I) Immunofluorescence images of GFP/YFP+ cells and KDR+ cells. Yellow arrowheads denote GFP/YFP+KDR+ cells and white arrows GFP/YFP+KDR- cells.
(J) Immunofluorescence images of GFP/YFP+ cells and HNF4A+ cells. Arrow denotes GFP/YFP+ cells with weak HNF4A staining.
Numerical data are presented as mean ± s.d. Two-tailed Student's t-test, *p< 0.05, **p< 0.01, ***p < 0.001, ****p<0.0001. See also Figure S5.

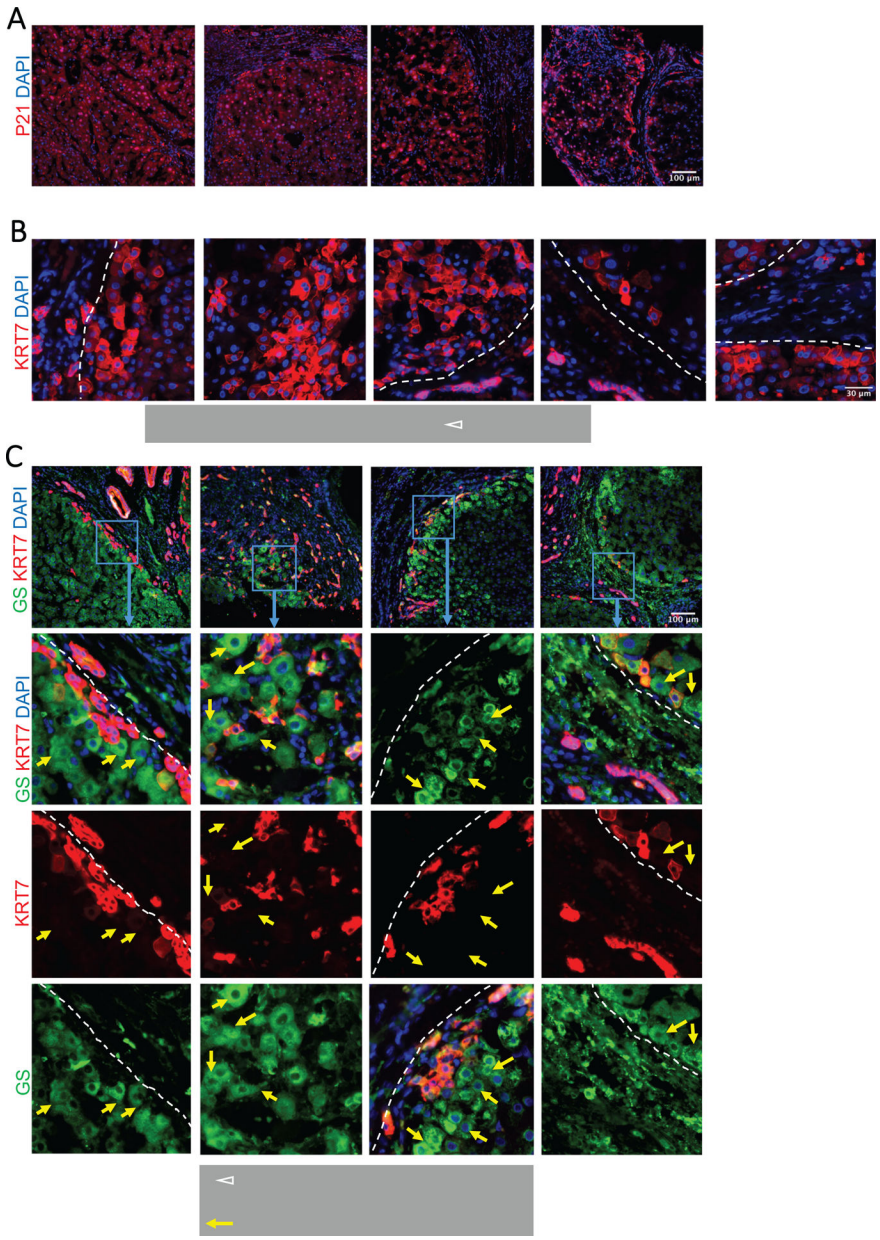

Figure 6. Evidence of BEC-to-hepatocyte conversion in human liver samples from nonalcoholic steatohepatitis (NASH) cirrhosis and alcoholic cirrhosis ESLD patients.

(A) Immunofluorescence images of p21 expression in 4 out of 5 human cirrhotic liver specimens.

(B) Immunofluorescence images of small cuboidal KRT7+ BECs (arrowheads) and KRT7+ intermediate hepatocyte-like cells (arrows) present in the regenerative nodules (*) close to the fibrous septa (outlined).

(C) Immunofluorescence images of KRT7+ and GS+ cells in human cirrhotic specimens. White arrowheads depict GS+KRT7+ BECs. White arrows depict the rare GS+KRT7+ intermediate hepatocyte-like cells and yellow arrows the GS+KRT7- intermediate hepatocyte-like cells. See also Figure S6 and S7.

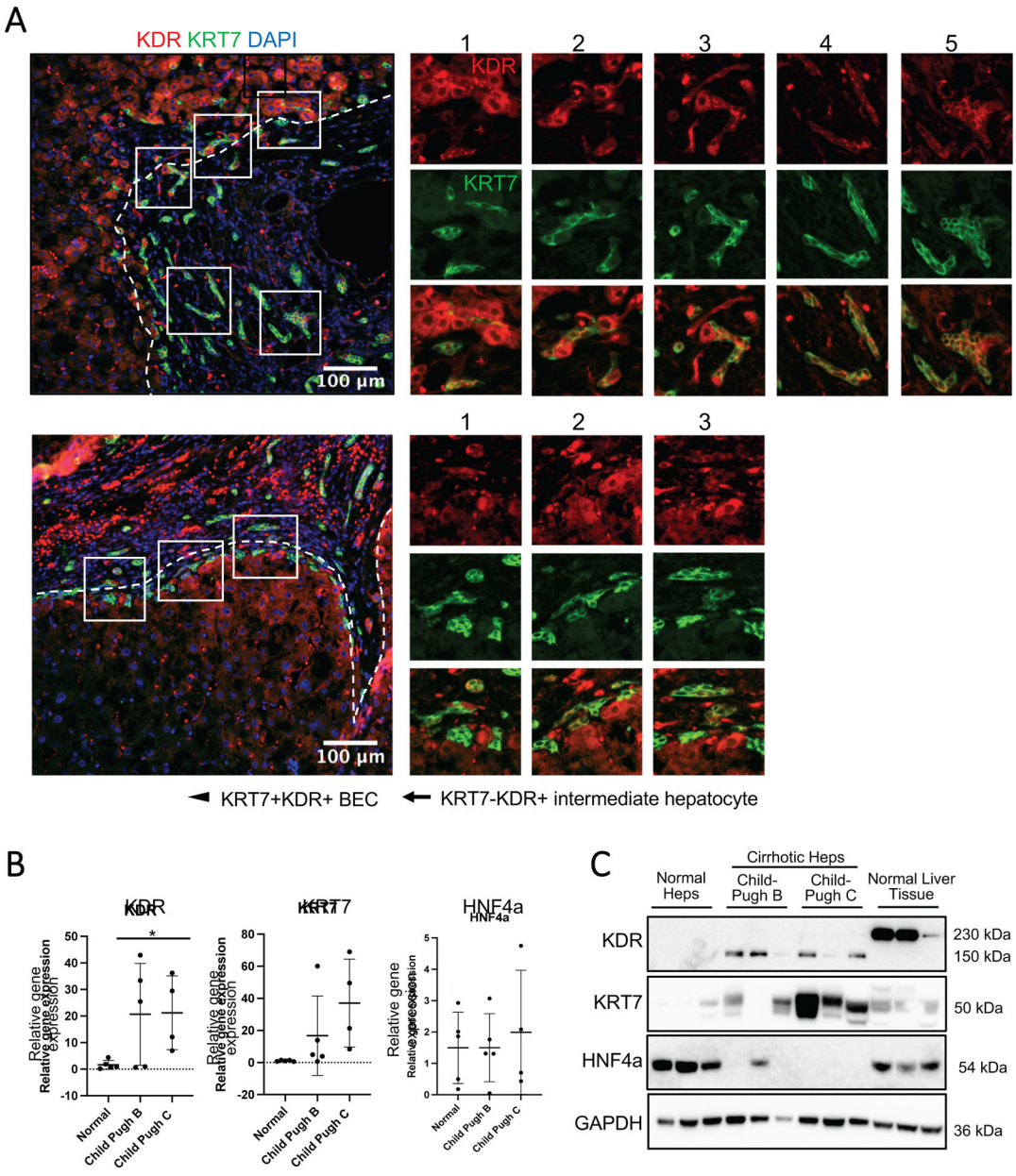

Figure 7. Evidence of KDR expression on BECs in human liver samples from non-alcoholic steatohepatitis (NASH) cirrhosis and alcoholic cirrhosis ESLD patients.

(A) Immunofluorescence images of cirrhotic liver specimens HH121 and HH125 showing fibrous septa stained for KRT7+ BECs and KDR+ sinusoidal endothelial cells. Note numerous KRT7+KDR+ BECs (arrowheads) and larger KDR+ intermediate hepatocyte-like cells (arrows) surrounding the KRT7+KDR+ BECs.

(B) Relative gene expression of *KDR*, *KRT7*, *HNF4A* in hepatocytes (Heps) isolated from normal (n=5) or cirrhotic human livers Child-Pugh B (n=5) and Child-Pugh C (n=4).

(C) Western blots showing protein expression of KDR, KRT7, HNF4A in hepatocytes isolated from normal or cirrhotic human livers Child-Pugh B (n=3) and Child-Pugh C (n=3) analyzed in panel D. GAPDH serves as endogenous control.

Numerical data are presented as mean ± s.d. Two-tailed Student's t-test for comparison between two groups, *p < 0.05. See also Figure S7.

Key Resources Table

REAGENT or RESOURCE	SOURCE	IDENTIFIER
Antibodies used in western blot		
HNF4A	Abcam	Cat#ab41898; RRID:AB_732976
KDR	Cell Signaling	Cat#2479s; RRID:AB_2212507
CD31	Abcam	Cat#aAb32457; RRID:AB_726369
KRT19	Progen	Cat#61029; RRID:AB_2920695
KRT7	Novus Biologicals	Cat#NBP2-44814
GAPDH	Proteintech	Cat#60004-1-Ig; RRID:AB_2107436
Antibodies used in tissue immunostaining		
RFP	Rockland	Cat#600-401-379S; RRID:AB_11182807
EpCAM	BD Biosciences	Cat#552370; RRID:AB_394370
KRT7	Abcam	Cat#ab181598; RRID:AB_2783822
KDR	Cell signaling	Cat#2479s; RRID:AB_2212507
HNF4A	Abcam	Cat#ab201460; RRID:AB_2927380
CD26	R&D Systems	Cat#AF954-SP; RRID:AB_355739
KRT19	Abbomax	Cat#602-670
YFP/GFP	Thermo Fisher Scientific	Cat#A10262; RRID:AB_2534023
GS	Thermo Fisher Scientific	Cat#MA5-27749; RRID:AB_2735204
Mouse p21	Abcam	Cat#ab188224; RRID:AB_2734729
CD31	BD Biosciences	Cat#557355; RRID:AB_396660
Human p21	Cell signaling	Cat#2947s; RRID:AB_823586
Antibodies used in flow cytometry		
APC anti-mouse CD45	Biolegend	Cat#103112; RRID:AB_312976
APC anti-mouse TER-119	Biolegend	Cat#116211; RRID:AB_313713
APC anti-mouse CD31	Biolegend	Cat#102409; RRID:AB_312904
APC anti-mouse/human CD11b	Biolegend	Cat#101211; RRID:AB_312794
BV605 Rat Anti-Mouse CD26	BD Biosciences	Cat#745125; RRID:AB_2742729
APC/Cyanine7 anti-mouse CD326 (EpCAM)	Biolegend	Cat#118217; RRID:AB_2098648
Rat anti-mouse CD16/32 (Fc Block)	BD Biosciences	Cat#553141; RRID:AB_394656
Oligonucleotides		
DNA sequences used as template to in vitro transcribe nucleoside modified mRNA, see Table S2	This paper	N/A
For primers used in Figures 7 and S7, see Table S3	This paper	N/A
Deposited data		
Sequence data	This paper	GEO: (https://www.ncbi.nlm.nih.gov/geo/query/acc.cgi?acc=GSE242847)
Experimental models: Organisms/strains		
Krt19-Cre^{ERT}	Jackson Laboratory	Cat# 026925
R26^{LSL}tdTomato	Jackson Laboratory	Cat# 007914

REAGENT or RESOURCE	SOURCE	IDENTIFIER
Kdr-2A-Cre^{ERT2}-2A-eYFP	This paper	N/A
Kdr^{tm2Sato}/J	Jackson Laboratory	Cat#018977
B6.129P2-Gt(ROSA)26Sor$^{tm1(CAG-Brainbow2.1)Cle}$*/j*	Jackson Laboratory	Cat# 017492
Transgenic zebrafish lines		
Tg(Tp1:H2B-mCherry)	[35]	*Tg(EPV.Tp1-Mmu.Hbb:hist2h2l-mCherry),* Allele s939
Tg(Tp1:VenusPEST)	[35]	*Tg(EPV.Tp1-Mmu.Hbb: Venus-Mmu.Odc1),* Allele s940
Tg(fabp10a:CFP-NTR)	[35]	*Tg(fabp10a:CFP-NTR),* Allele s931
Tg(hs:sflt1)	[51]	*Tg(hsp70l:flt1,cryaa:Cerulean),* Allele bns80
Tg(Tp1:CreERT2)	[35]	*Tg(EPV.Tp1 -Mmu.Hbb:Cre-ERT2,cryaa:mCherry),* Allele s959
Tg(hs:loxP-mCherry-loxP-hVEGFA)	[48]	*Tg(hsp70l:LOXP-mCherry-LOXP-Hsa.VEGFA,Xla.Cryg:EGFP),* Allele mn32
Tg(hs:hVEGFA-P2A-Venus)	This study	*Tg(hsp70l:Hsa. VEGFA165-P2A -Venus,Xla. CrygECFP),* Allele pt624
Critical commercial assays		
hVEGFA ELISA Kit	Abcam	Cat# ab119566
PAS Staining kit	Sigma Aldrich	Cat# 395B
Trichrome Staining kit	Abcam	Cat# ab150686
Total Cholesterol kit	FUJIFILM Wako Diagnostics	Cat# 999-02601
Click-iT™ Plus TUNEL Assay Alexa Fluor™ 488 dye	Invitrogen	Cat# C10617
Click-iT™ EdU Alexa Fluor™ 488 Imaging KiT	Invitrogen	Cat# C10337
Click-iT™ Plus EdU Cell Proliferation Kit for Imaging, Alexa Fluor™ 647 dye	Invitrogen	Cat# C10640
Alexa Fluor™ 594 Tyramide SuperBoost™ Kit	Invitrogen	Cat# B40944
RevertAid First Strand cDNA Synthesis Kit	Thermo Scientific	Cat# K1621
SYBR Green PCR Master Mix	Applied Biosystem	*Cat#* 4309155
Software and algorithms		
Image J version 2.3.0/1.53f	NIH	http://imagej.nih.gov/ij
Seurat v3.2.3	Satija Lab	https://github.com/satijalab/seurat
GraphPad Prism 10.0.2	Graphpad Prism Software	https://www.graphpad.com/scientific-software/prism/
FlowJo Software v.10.8.1	Becton Dickinson & Company	https://www.flowjo.com/solutions/flowjo